Biomedicine & Pharmacotherapy 174 (2024) 116517

Contents lists available at ScienceDirect

Biomedicine & Pharmacotherapy

journal homepage: www.elsevier.com/locate/biopha

Equisetum arvense standardized dried extract hinders age-related osteosarcopenia

Laura Salvadori [a,b], Martina Paiella [a,b], Beatrice Castiglioni [c], Maria Laura Belladonna [d], Tommaso Manenti [e], Catia Ercolani [e], Luca Cornioli [e], Nausicaa Clemente [f], Andrea Scircoli [a,b], Roccaldo Sardella [g], Leonardo Tensi [g], Andrea Astolfi [g], Maria Letizia Barreca [g], Sara Chiappalupi [b,d], Giulia Gentili [b,d], Michela Bosetti [c,1], Guglielmo Sorci [b,d,1], Nicoletta Filigheddu [a,b,1], Francesca Riuzzi [b,d,*,1]

[a] *Department of Translational Medicine, University of Piemonte Orientale, Novara 28100, Italy*
[b] *Interuniversity Institute of Myology (IIM), Perugia 06132, Italy*
[c] *Department Pharmaceutical Sciences, University of Piemonte Orientale, Novara, Italy*
[d] *Department of Medicine and Surgery, University of Perugia, Perugia 06132, Italy*
[e] *Laboratori Biokyma srl, Anghiari, Arezzo 52031, Italy*
[f] *Department of Health Sciences and Interdisciplinary Research Center of Autoimmune Diseases (IRCAD), University of Piemonte Orientale, Novara 28100, Italy*
[g] *Department of Pharmaceutical Sciences, University of Perugia, Perugia 06123, Italy*

ARTICLE INFO

Keywords:
Muscle atrophy
Osteoclastogenesis
Natural compounds
Target fishing

ABSTRACT

Age-associated osteosarcopenia is an unresolved syndrome characterized by the concomitant loss of bone (osteopenia) and skeletal muscle (sarcopenia) tissues increasing falls, immobility, morbidity, and mortality. Unbalanced resorption of bone in the remodeling process and excessive protein breakdown, especially fast type II myosin heavy chain (MyHC-II) isoform and myofiber metabolic shift, are the leading causes of bone and muscle deterioration in the elderly, respectively. *Equisetum arvense* (*EQ*) is a plant traditionally recommended for many pathological conditions due to its anti-inflammatory properties. Thus, considering that a chronic low-grade inflammatory state predisposes to both osteoporosis and sarcopenia, we tested a standardized hydroalcoholic extract of *EQ* in *in vitro* models of muscle atrophy [C2C12 myotubes treated with proinflammatory cytokines (TNFα/IFNγ), excess glucocorticoids (dexamethasone), or the osteokine, receptor activator of nuclear factor kappa-B ligand (RANKL)] and osteoclastogenesis (RAW 264.7 cells treated with RANKL). We found that *EQ* counteracted myotube atrophy, blunting the activity of several pathways depending on the applied stimulus, and reduced osteoclast formation and activity. By *in silico* target fishing, IKKB-dependent nuclear factor kappa-B (NF-κB) inhibition emerges as a potential common mechanism underlying *EQ*'s anti-atrophic effects. Consumption of *EQ* (500 mg/kg/day) by pre-geriatric C57BL/6 mice for 3 months translated into: i) maintenance of muscle mass and performance; ii) restrained myofiber oxidative shift; iii) slowed down age-related modifications in osteoporotic bone, significantly preserving trabecular connectivity density; iv) reduced muscle- and spleen-related inflammation. *EQ* can preserve muscle functionality and bone remodeling during aging, potentially valuable as a natural treatment for osteosarcopenia.

Abbreviations: Akt, protein kinase B; BS, bone surface; BV, bone volume; Cb, cortical bone zone; Cbt, cortical bone thickness; CnAr/ TV, cancellous bone area/tibia volume; Conn. D, connectivity density; CSA, cross-sectional area; Dex, dexamethasone; *EQ*, *Equisetum arvense*; FI, fusion index; GC, gastrocnemius; IFN-γ, interferon-γ; IκB, IkappaB kinase; IKKB, protein Kinase-1-mediated IκB Kinase β; MAPK, mitogenic activated protein kinase; METz, metaphyseal zone; mTOR, mammalian target of rapamycin; MyHC-II, type II myosin heavy chain; NF-κB, nuclear factor kappa-light-chain-enhancer of activated B cells; NpM, nuclei per myotube; OB, osteoblast; OC, osteoclast; PPAR-γ, peroxisome proliferator-activated receptor gamma; RSK1, p90 ribosomal S6 kinase 1; OS, osteosarcopenia; QF, *quadriceps femoris*; RANKL, receptor activator of nuclear factor kappa-B ligand; TA, *tibialis anterior*; Tb, trabeculae; Tb.N, trabecular number; Tb.Th, trabecular thickness; TNF-α, tumor necrosis factor-α; TRAP, tartrate-resistant acid phosphatase.

* Corresponding author at: Interuniversity Institute of Myology (IIM), Perugia 06132, Italy.
E-mail address: francesca.riuzzi@unipg.it (F. Riuzzi).
[1] Shared senior authorship.

https://doi.org/10.1016/j.biopha.2024.116517
Received 18 January 2024; Received in revised form 20 March 2024; Accepted 28 March 2024
Available online 3 April 2024

1. Introduction

Osteoporosis and sarcopenia are characterized by deterioration of bone microarchitecture and by progressive and extensive loss of skeletal muscle mass, respectively, compromising their functionality [1,2]. The imbalance between osteoclast (OC; bone-resorbing cells) and osteoblast (OB; bone-reforming cells) activity is the main cause of osteoporosis, whereas sarcopenia is principally due to the reduction of the protein synthesis in conjunction with an increase of protein breakdown, especially of the myofibrillar protein myosin heavy chain (MyHC). A metabolic shift of type II glycolytic (fast-twitch) towards type I oxidative (slow-twitch) fibers in muscle also occurs during aging [3]. Alarmingly, elderly people in Western countries are predisposed to the coexistence of osteoporosis and sarcopenia leading to a new concept of "osteosarcopenia" (OS) as a unique geriatric syndrome [1,4]. Indeed, bone and muscle are anatomically and metabolically linked, communicating each other through osteokines and myokines. The altered presence of these small molecules during aging disrupts the physiological bone-muscle crosstalk contributing to the synchronous degeneration of both tissues in OS, leading to an increased number of falls, bone fractures, hospitalizations and thus a reduction in quality of life [5,6]. Sarcopenia and osteoporosis also share risk factors and pathogenesis, including the chronic low-grade inflammatory status known as "inflammaging" [1–6]. Currently, efficacious therapies acting concomitantly on both sarcopenia and osteoporosis are unavailable. Physical activity combined with protein supplementation and the treatment with the anti-osteoporosis drug Denosumab showed partial beneficial effects on the muscle-bone unit in OS conditions [1]. However, this approach is not applicable in fragile elderly subjects, encouraging further investigation on therapeutic strategies simultaneously targeting muscle and bone tissues.

Due to their bioactive compound content, many phytoextracts have been investigated to counteract multiple diseases. *Equisetum arvense* (*EQ*), commonly known as horsetail, is a perennial fern with green and sterile stems representing the plant's drug. Hepatoprotective, diuretic, anti-bacterial, anti-inflammatory, and antioxidative properties have been assigned to *EQ* in virtue of its flavonoid content. Since *EQ* is the terrestrial plant with the highest concentration of silicates (5–8% of the dry herb), calcium, potassium, and other minerals [7], it is traditionally used to prevent osteoporosis around the World, and it is mentioned in the European Pharmacopoeia for its ability to increase bone and cartilage formation and strengthen bones. However, scientific evidence is not enough to declare *EQ* as bone-protecting in clinical practice [8] and the role of *EQ* in muscle homeostasis and sarcopenia has not been investigated so far. Since inflammaging is a crucial mechanism in both sarcopenia and osteoporosis conditions, we assessed the potential beneficial effects of *EQ* in OS. To this aim, we used several *in vitro* models as well as geriatric mice. The molecular mechanisms underpinning the effects of *EQ* and the potential active compounds were uncovered.

2. Material and methods

2.1. Reagents and resources

See Supporting Information.

2.2. Equisetum arvense (EQ) standardized dried extract

We used a standardized dried extract of *Equisetum arvense* L. with 10% (w/w) minimum silica content established by thin-layer chromatography (TLC). The extract was bought from A.C.E.F. spa, Italy, lot nr: N23240N1. *Equisetum arvense* L. was harvested during the period of June-August 2019. After the conformity assessment of raw material to the food grade requirements, the entire herb extract was extracted by a water/ethanol (80/20 v/v) solution, with an approximate DER (Drug Extract Ratio) of 8–1. The dry extract of *Equisetum* was then made by spray-drying technique in a maltodextrin-based matrix.

2.3. Ultra-high performance liquid chromatography-tandem mass spectrometry (UHPLC-MS/MS)

Liquid chromatographic separation and mass spectrometric analysis were performed on a UHPLC-MS/MS system consisting of an Agilent 1290 Infinity II combined with the Agilent 6560 mass spectrometer (Agilent Technologies Inc., Santa Clara, California, United States). The chromatographic separation was performed using a ZORBAX RRHD Eclipse Plus C18 column (50 mm×2.1 mm, 1.8 μm, 95 Å, Agilent Technologies Inc.). UHPLC eluent A was water (LC-MS grade, LiChrosolv, Supelco) with 0.1% (v/v) formic acid (LC-MS grade, LiChropur, Supelco) while eluent B was acetonitrile (LC-MS grade, LiChrosolv, Supelco). The optimized gradient program was the following: 0–2.5 min, 5% (v/v) B; 2.5–4 min, 5–25% (v/v) B; 4–7 min, 25–35% (v/v) B; 7–9.5 min, 35–97% (v/v) B; 9.5–10.5 min, 97% (v/v) B; 10.5–11 min, 97–5% (v/v) B; 11–16 min, 5% (v/v) B (column equilibration/conditioning). The column temperature was set at 30 °C and the flow rate at 0.3 mL min^{-1}. The injection volume was 5 μL. The UV-Vis chromatograms were recorded at 250, 280, 320, and 350 nm. For MS detection, the Dual AJS ESI source operated in positive ion mode. The Gas temperature was set at 300 °C with a flow of 5 L min^{-1} while the Sheath Gas Temperature was 350 °C with a flow of 11 L min^{-1}. The nebulizer pressure was set at 35 psi and the Capillary and Fragmentor voltages were 3500 V and 300 V, respectively. In the case of MS^2 analysis, multiple experiments using the iterative algorithm of the instruments were carried out. The fragmentation patterns of the compounds were recorded at a fixed collision energy (20 eV) with an isolation width of 4 *m/z*. The Masshunter Workstation Data Acquisition 10.0 (Agilent Technologies Inc., Santa Clara, California, United States) program was used for data acquisition while the Masshunter Qualitative Analysis 10.0 (Agilent Technologies Inc., Santa Clara, California, United States) software was used for data processing.

2.4. Cell cultures and treatments

Murine C2C12 myoblasts were cultured in Dulbecco's Modified Eagle's Medium (DMEM) containing high glucose (4500 mg/L) and supplemented with 20% fetal bovine serum (FBS), 100 U/mL penicillin and 100 mg/mL streptomycin (P/S) (growth medium, GM). Myotubes were obtained by shifting sub-confluent myoblasts to DMEM supplemented with 2% horse serum (HS) (differentiation medium, DM) for 4 days [9]. *EQ* (25–600 μg/mL) was added to myoblasts or to preformed myotubes in the absence or presence of recombinant tumor necrosis factor (TNF)-α (20 ng/mL) plus interferon (IFN)-γ (100 U/mL), dexamethasone (Dex; 1 μM), or receptor activator of nuclear factor kappa beta (RANKL; 100 ng/mL), for the indicated time. Pre-treatment with BAY11–7082 (10 μM) for 30 min was used to inhibit NF-κB (nuclear factor kappa-light-chain-enhancer of activated B cells).

The murine macrophage cell line RAW 264.7 was cultured in RPMI-1640 supplemented with 10% FBS, 2 mM L-glutamine and P/S. To induce differentiation in OCs, cells were treated with RANKL (100 ng/mL) for 5 days, in the absence or presence of *EQ* (12.5–400 μg/mL), refreshing the culture medium every third day [10,11].

2.5. May-Grünwald/Giemsa staining

The cells were fixed and processed as previously described [12]. The images were acquired (Olympus IX51) at 4× or 10× magnification.

2.6. Immunofluorescence (IF) for MyHC-II expression

Myotubes cultivated on sterile glass coverslips were fixed and processed as previously described [9] by using mouse anti-MyHC-II primary and anti-mouse Alexa Fluor 488-conjugated antibodies. Nuclei were visualized with DAPI (4′,6-diamidino-2-phenylindole). Coverslips were mounted with a fluorescent mounting medium and viewed with an

epifluorescence microscope (Leica DMRB) equipped with a digital camera.

2.7. Cell viability by MTT 3-(4,5-dimethylthiazol-2-yl)-2,5-diphenyltetrazolium bromide assay

C2C12 myotubes and OCs were incubated with 110 μL of medium containing MTT 50 μg. After 4 h, solubilization buffer (SDS 10% in HCl 0.01 M) was added to each well, and absorbance at 570 nm was measured using a UV/visible spectrophotometer (TECAN, Thermo Fisher Scientific, Waltham, MA, USA).

2.8. TRAP (tartrate-resistant acid phosphatase) staining and activity

OCs were stained with TRAP reagent and images were acquired by a bright-field light microscope (Olympus IX51) at 10× magnification. TRAP-positive multinucleated cells with three or more nuclei were considered OCs and were counted in randomly selected visual fields of each well using Image J software (Table S1). As previously described, TRAP activity was assayed in 30 μL of harvested supernatants [10,11,13]. Absorbance at 540 nm was measured using a UV/visible spectrophotometer (TECAN, Thermo Fisher Scientific, Waltham, MA, USA).

2.9. F-actin ring-formation assay

OCs were fixed with 4% PFA for 20 min and stained with 10 μg/mL rhodamine-conjugated phalloidin for 60 min at 37°C. Nuclei were stained with DAPI. The samples were viewed with an epifluorescence microscope (Leica DMRB) equipped with a digital camera. The number of OCs was counted as previously described [13].

2.10. Animal models

The dry extract of *EQ* was dissolved in water and administered at the dose of 500 mg/kg/die to 21-month-old male and female C57BL/6 mice (*EQ* Old; n=10), while the control group did not receive any treatment (Untr. Old; n=8). Adult (6-month-old) male (n=3) and female (n=3) mice were used as controls. Based on previous studies measuring the primary outcome of the present work (*i.e.*, age-dependent skeletal muscle weight loss), at least 6 mice per group were estimated to be sufficient to detect a relative difference of about 30% in the means of *EQ*-treated vs. untreated mice assuming an SD of 0.04, an 80% power, and a type I error p=0.05. After three months, animals were sacrificed, and hindlimb muscles, spleens, and inguinal and epididymal adipose tissues were surgically excised and weighed. The tibia and femur were removed and immediately frozen in liquid nitrogen. Animal procedures followed the 3Rs principles in alignment with Directive 2010/63/EU of the European Union and approved by the Ethics Committee of Perugia University and the Italian Ministry of Health. Mice were housed under specific pathogen-free conditions on a 12 h light/day cycle and raised under a standard mouse diet.

2.11. Kondziela's inverted screen test

Twice a week during the three months, each mouse was placed in the center of a wire mesh screen, which was gently overturned by 180°, and the time when the mouse falls off, was recorded for a maximum of 8 min. The test was repeated three times with 10 min inter-trial intervals for each mouse [9].

2.12. Western blotting

Samples were lysed in a protein extraction buffer [9] and equal amounts of total protein extract (20–30 μg) were resolved by SDS-PAGE (Sodium Dodecyl Sulfate-PolyAcrylamide Gel Electrophoresis) and transferred to 0.45 μm nitrocellulose blots. Following blocking with 5% non-fat dried milk primary and secondary antibodies were applied as indicated in Table S1. The immune reactions were developed by enhanced chemiluminescence and acquired by the C-DiGit Blot Scanner (LI-COR, USA).

2.13. Real-time PCR

RNA extraction, reverse transcription, and real-time PCR analyses of mRNA contents were performed as previously described for cellular and organ samples [9]. The primers and software used for real-time PCR analysis are reported in Tables S2 and S1, respectively. Bones were pestled in a liquid nitrogen-cooled mortar to lyse in RNAzol. RNA was retro-transcribed with High-Capacity cDNA Reverse Transcription Kit, and real-time PCR was performed using the TaqMan assays, *Col1a1* (Mm00801666_g1) and *Gapdh* (Mm99999915_g1) as the housekeeping gene.

2.14. Histology, immunohistochemistry (IHC), and IF

Muscles and spleens were formalin-fixed and paraffin-embedded. Four-μm cross-sections were obtained and processed for hematoxylin/eosin staining (H&E), IHC or IF [9]. Antibodies and dilutions are reported in Table S4. Not disarticulated femur and tibia of the left hindlimb were fixed for 2 days in PFA and embedded in 80% (v/v) methyl methacrylate (MMA) stabilized with benzoyl peroxide and placed in capped 5 mL glass vials at 37°C overnight for at least 3 days [14]. After the polymerization, the glass vials were broken, and moistened sections (80 μm) were cut on a Leica SP 1600 Saw Microtome with a rotating diamond saw blade for high-quality sample preparation of hard materials for microscopical analysis. Cuts were done on the long axis of the femur and tibia and the sections were stained using H&E or Fuchsin Light Green for histological evaluation. The prepared sections were examined morphologically and morphometrically by an investigator blinded to the identity of the material.

2.15. Morphometric evaluations

Morphometric evaluations were performed by using Image J software. Myotube areas, fusion index (FI, number of nuclei in myotubes containing minimum 3 nuclei/total number of nuclei), and nuclei per myotube (NpM) were calculated on images of May-Grünwald/Giemsa as previously described [12]. FI was calculated as × 100 in 5 randomly selected fields per well. NpM were counted in 50 randomly chosen myotubes. Myotube diameters were determined after IF MyHC-II staining at 20× magnification as previously described [12]. Average diameters of at least 100 myotubes from 10 randomly chosen fields for each condition were determined. The width of each myotube was measured at 3 different points along the longitudinal axis of the cell.

Slices were analyzed and photographed with a bright field microscope (Olympus BX51) equipped with a digital camera to measure myofiber cross-sectional area (CSA), centrally nucleated, and MyHC-slow and -fast myofibers on total sections at 100 μm intervals for each muscle.

The bone morphometric analysis was performed using a semi-automatic image analyzer (GIPS Image processing software for the I.T.I. PCV board) connected to a Leitz Laborlux S light microscope. The bone structure, resorption, and mass were measured in the cortical or under the metaphyseal (Metz) regions of the tibia of female C5/BL/6 mice. The thickness of the cortical bone was measured in the tibias' mid-shaft region through twenty-five random linear measurements of cortex thickness in 2 mm length of tibia diaphysis for each animal studied. Cancellous bone area (CnAr) was estimated for bone resorption in the upper tibiae under the growth plate and without considering it or in the epiphyseal region, through semiautomatic image delineation of green trabecular area in fuchsin fast green stained bone. All measurements were performed at 4× or 20× magnification respectively for cortical

thickness or trabecular areas and done by two blinded investigators by Image J software (Table S1).

2.16. Micro-CT analysis

Femur and tibia were fixed with 4% PFA for Quantum GX2 micro-CT Imaging System (PerkinElmer, Massachusetts, USA) analysis by using the following parameters: 90 kV tube potential, 88 μA X-ray tube current, 0.5 mm Al filter, 0.4° rotation step, 5 μm^3 size isotropic voxel, 4 min exposure time, 14 min collection time, 18 mm visual field and 36μm pixel size. Each leg was rotated 360° to obtain the data, which were entered into the analyzing software (Table S1) to reconstruct 3D images of distal femurs and proximal tibiae. To measure bone microarchitecture parameters proximal tibiae was selected and the epiphysis or growth plate was excluded from the analysis; the growth plate plus 0.2 mm was used as a structural reference among samples and 1 mm region of thick was selected. The trabecular and the cortical parts were separated with semi-automatically drawn contours and 3D parameters *i.e.*, bone volume (BV), bone surface area (BS), trabecular thickness (Tb.Th), trabecular number (Tb.N), and trabecular connectivity density (Conn. D) were calculated and expressed according to American Society for Bone and Mineral Research (ASBMR) recommendations [15].

2.17. In silico target fishing

The 2D structure of compounds **1-15** were retrieved from PubChem (https://pubchem.ncbi.nlm.nih.gov/) and prepared by using the LigPrep [16] to produce low energy 3D structures taking into account the ionization states, stereochemistry, the tautomerism, and ring conformations at the desired pH (7.5 ± 0.5). As protein model, the structure of IKKB co-crystallized with K252a (PDB ID: 4KIK) was downloaded from RCSB PDB [17] and prepared using Schrödinger's Protein Preparation Workflow (Schrödinger Release 2024–1) [18–21] to obtain satisfactory starting structures for the docking studies. The complex was pre-processed as follows: i) hydrogen atoms were added and bond orders were assigned to amino acid residues and ligands; ii) the missing side chains were filled; iii) the protein was capped with acetyl (ACE) and N-methylamine (NMA) groups; iv) all water molecules beyond 3 Å from heteroatoms were deleted; and v) Epik (Schrödinger Release 2024–1) [19] was used to predict the ionization and tautomeric states for the ligands (pH = 7.0 ± 2). Then, the H-bond network of the complex was optimized using PROPKA for the assignment of the residue protonation states (pH = 7.0). Finally, the complex was submitted to a restrained minimization (OPLS4 force field [22]), which was stopped when the RMSD of heavy atoms reached 0.30 Å.

Docking studies were performed using Schrödinger's Glide software (Schrödinger Release 2024–1) [23,24]. In our protocol, the crystallographic position of K252a (PDB ID: 4KIK) was used as a reference to center the grid. The docking space was defined as a cubic box (24 Å outer box), with an inner cubic box (10 Å) defining the region where the centroid of the ligand had to be located. The centroid for the 4KIK protein had coordinates of 48.35, 29.97, and −56.52 to the x-, y-, and z-axis, respectively. After grid preparation with the "receptor grid generation" tool, docking experiments were performed using the Glide SP (Standard Precision) protocol. For each ligand, the poses generated during the docking simulations were clustered using a root mean square deviation threshold of 1.5 Å and a maximum atomic displacement threshold of 2.3 Å. Finally, one pose for each ligand was retained.

2.18. Statistical analysis

Quantitative data are presented as means ± SD (standard deviation) or SEM (standard error of the mean) of at least three independent experiments. Counts were performed by three independent operators blind to the treatments. Representative experiments and images are shown unless stated otherwise. Statistical analysis was performed using the ANOVA one-way analysis or two-tailed, unpaired *t*-test when appropriate. The IC_{50} values were calculated by non-linear regression method [log(inhibitor) vs. response—Variable slope] using GraphPad Prism Version 8.0.1 software. P values <0.05 were considered statistically significant. Statistical analyses were performed using R Studio software or Prism GraphPad (Table S1).

3. Results

3.1. Equisetum arvense (EQ) protects myotubes against multiple atrophying stimuli and promotes myoblast differentiation and fusion into myotubes

Treatment of C2C12 myotubes with *EQ* (6.25–800 μg/mL) in the absence of atrophying stimuli reduced cell viability at the highest dose used (400 and 800 μg/mL) (Fig. S1A) without affecting preformed myotube diameter and MyHC-II expression (Fig. S1B, C), suggesting that highest doses of *EQ* might exert toxic effects in non-fused myoblasts present in the culture.

Preformed myotubes treated with TNFα/IFNγ (T/I) or dexamethasone (Dex) are well-characterized *in vitro* models of atrophy in which a pronounced and selective degradation of MyHC-II is induced [25]. Indeed, we found that T/I reduced myotube area by ~60%, and the addition of *EQ* significantly counteracted this effect starting from 25 μg/mL and with the highest efficacy at 100 μg/mL (Fig. S2A). Based on the dose-dependent *EQ* atrophy-protective effect observed within the five lowest tested doses (EC_{50}=58.88 μg/mL), *EQ* 100 μg/mL was selected for further investigation (Fig. S2B). We found that *EQ* 100 μg/mL abolished the T/I-induced reduction of myotube diameters (Fig. 1A) and MyHC-II expression (Fig. 1B). Interestingly, higher 200 μg/mL concentrations were not efficacious in inhibiting the T/I atrophic effect resulting in a bell-shaped dose-response curve (Fig. S2C), as reported for other natural extract activities [26].

Similarly to T/I, Dex treatment reduced myotube diameters and MyHC-II content, and the addition of *EQ* hampered the glucocorticoid's atrophying effect (Fig. 1C,D). *EQ* preserved myotube size and MyHC-II expression also in the presence of atrophying amounts of receptor activator of nuclear factor kappa-B ligand (RANKL) (Fig. 1E,F), a chemokine that activates RANK pathway sustaining the pathogenesis of osteoporosis, with implication in sarcopenia [27].

Finally, *EQ* exerted direct effects on myoblasts since C2C12 cells cultured in DM in the presence of *EQ* showed i) increased myotube total area, fusion index (FI), and number of nuclei per myotube (NpM) at 72 h (Fig. S3A,B); ii) strong activation of the pro-myogenic p38 mitogen-activated protein kinase (MAPK) [28] at 48 h (Fig. S3C); and, iii) increased expressions of the terminal differentiation markers, myogenin and MyHC-II, at 72 h and 6d, respectively (Fig. S3C).

3.2. EQ preserves protein content affecting different pathways depending on the applied atrophying stimulus and inhibiting NF-κB as a common mechanism

To unravel the molecular mechanism(s) underpinning the anti-atrophic effect of *EQ*, we investigated pathways known to be affected by T/I or Dex [28–30], the mechanism used by RANKL being poorly understood [31]. We confirmed the T/I- and Dex-dependent phosphorylation (activation) of catabolic p38 MAPK, NF-κB(p65), and signal transducer and activator of transcription 3 (STAT3), the deactivation of the anabolic protein kinase B (Akt)/mammalian target of rapamycin (mTOR) axis, and reduced MyoD levels [28] (Fig. 2A,B). *EQ* selectively counteracted the activation of p38 MAPK, NF-κB(p65), and STAT3 induced by T/I, and the activation of NF-κB(p65) and Akt/mTOR axis induced by Dex (Fig. 2A,B). Moreover, *EQ* blunted the Dex-induced ubiquitin-proteasome system (UPS)-dependent proteolysis by restraining the upregulation of the atrogene *Trim63* (muscle RING finger-1; MuRF-1), and its upstream transcription factor *Foxo3* (forkhead box

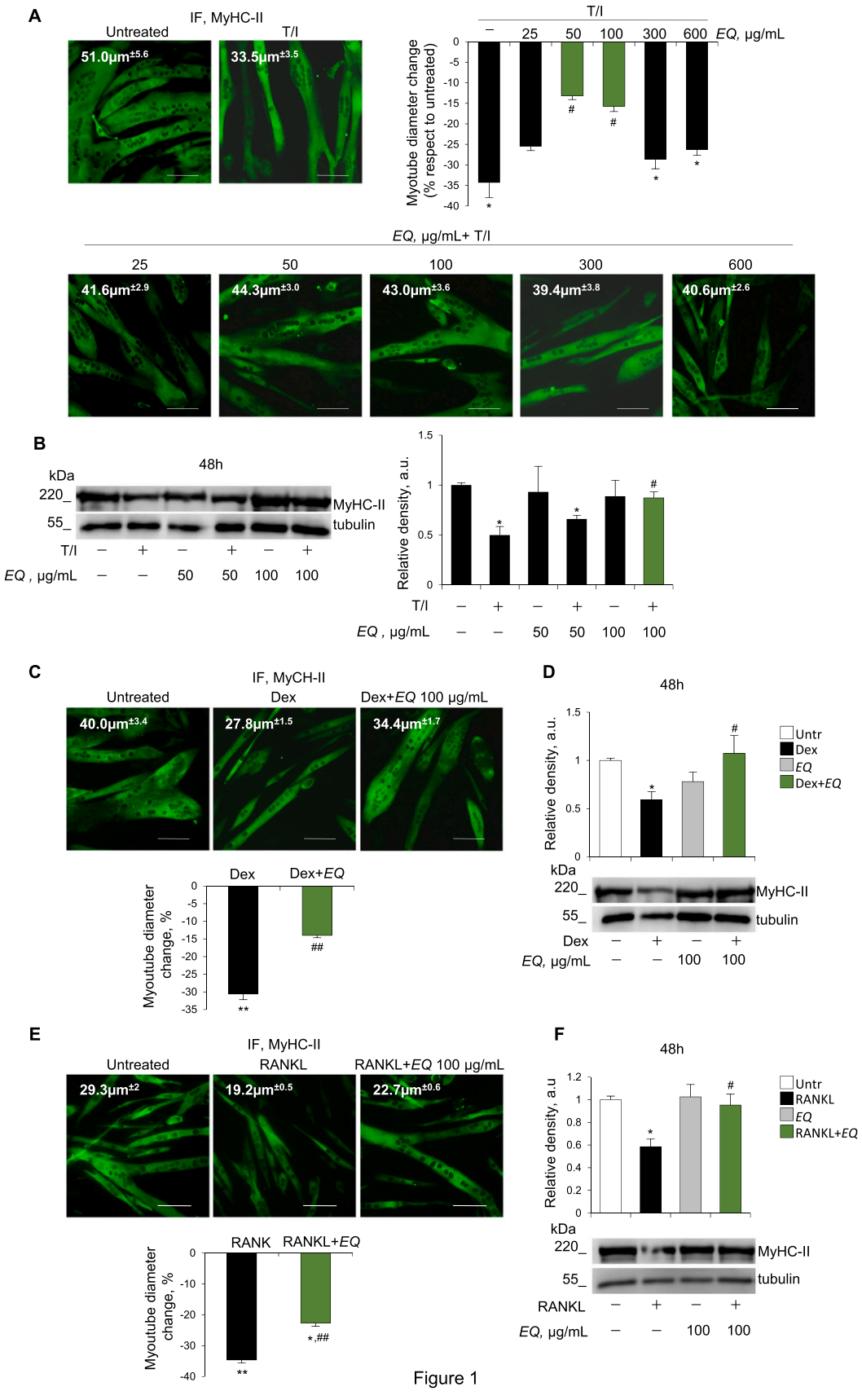

Figure 1

(caption on next page)

Fig. 1. *Equisetum arvense* (*EQ*) extract counteracts myotube diameter decrease and myosin heavy chain (MyHC)-II degradation induced by different atrophying stimuli. (A-F) Myotubes obtained by culturing C2C12 myoblasts in differentiation medium (DM) for 4 days were treated with TNFα (tumor necrosis factor α, 20 ng/mL)/IFNγ (interferon γ, 100 U/mL) (T/I) (A,B), dexamethasone (Dex, 1 μM) (C,D) or receptor activator of nuclear factor kappa-B ligand (RANKL, 100 ng/mL) (E,F) in the absence or presence of *EQ* at the indicated doses (A,B) or 100 μg/mL (C-F) for 48 h. (A,C,E). Immunofluorescence (IF) analysis for MyHC-II was performed, and myotube diameters were measured by *Image J* software. Reported are values (μm) and percentage changes of myotube diameters *vs* untreated controls. (B,D,F) Western blotting (WB) analysis for MyHC-II was performed, and relative densities were calculated with respect to tubulin. Reported are representative images (A-F). The green bars represent the doses of *EQ* with significant effects. Results are the means ± standard error of the mean. Statistical analysis was conducted using the two-tailed *t*-test. * $p<0.05$ and ** $p<0.01$, significantly different from untreated control; # $p<0.05$ and ## $p<0.01$, significantly different from T/I, Dex, or RANKL. Scale bars (A,C,E), 100 μm.

O3) (Fig. 2C). Treatment with RANKL did not interfere with Akt/mTOR and STAT3 pathways (Fig. S4), while it translated into activation of p38 MAPK and NF-κB(p65) (Fig. 2D), and upregulation of the atrogenes, *Trim63* and *Fbxo32* (atrogin-1) (Fig. 2E). *EQ* abolished RANKL's effects completely (Fig. 2D,E). In the absence of atrophying stimuli, *EQ* did not modulate the investigated kinases (Figs. 2 and S3), in line with the inability of *EQ* to affect myotube size and MyHC-II expression in basal conditions (Fig. S1).

NF-κB activation emerged as the common mechanism inducing myotube catabolism (Fig. 2A,B,D), and a target of the *EQ*'s antiatrophic activity. Pre-treatment with the NF-κB inhibitor, BAY11–7082 strongly hampered the effects of T/I, Dex or RANKL in reducing myotube diameters, at a comparable extent to that observed with *EQ* (Fig. S5A,B,D).

Interestingly, BAY11–7082 completely or partially abolished the upregulation of *Fbxo32* and *Trim63* (Fig. S5E) induced by RANKL or Dex (Fig. S5C), respectively, suggesting that NF-κB is a major inducer of atrogenes in RANKL-treated myotubes. In contrast, Dex might use several pathways to induce its atrophying effects [30,32].

Finally, *EQ* counteracted the T/I-, Dex- or RANKL-induced reduction in NpM (Fig. S6), suggesting that in the presence of atrophying stimuli *EQ* might sustain the myogenic potential of muscle precursor cells, which might contribute to slowing down the loss of muscle mass during aging [3].

3.3. *EQ inhibits RANKL-induced osteoclastogenesis*

EQ is suggested for the treatment of osteoporosis thanks to its very high silica content which helps in the absorption and use of calcium and collagen synthesis, which is essential in the bone remodeling process [33]. Although the ability of *EQ* to improve OB function has been broadly investigated [7,8], the mechanisms underlying the effects of *EQ* in osteoclastogenesis are still unknown [9,12]. *EQ* increased the viability of RANKL-treated RAW 264.7 cells, demonstrating the absence of toxicity (Fig. S7A). Tartrate-resistant acid phosphatase (TRAP) staining, which allows identifying osteoclasts (OCs) as purple-pink multinucleated (≥3 nuclei) cells, showed that RANKL-dependent OC formation was significantly reduced by *EQ* (12.5–400 μg/mL) in a dose-dependent manner starting from 25 μg/mL (Fig. 3A), with a maximum inhibition at 200 μg/mL (IC_{50}=40.93±5.9 μg/mL) (Fig. 3B). In accordance, *EQ* drastically reduced the number of big (>3 nuclei) but not small (3 nuclei) OCs with intact-structured F-actin rings (Fig. S7B,C), which are indispensable for OC adhesion to the matrix and subsequent bone resorption [27,34].

Moreover, *EQ* dose-dependently prevented both RANKL-induced TRAP enzymatic activity (Fig. 3C) and upregulation of the osteoclastogenic markers, *Acp5* (acid phosphatase 5, tartrate resistant; TRAP), *Calcr* (calcitonin receptor), *Mmp9* (matrix metallopeptidase 9), and *Ctsk* (cathepsin K) (Fig. 3D) [11].

3.4. *EQ counteracts the loss of muscle mass and performance in geriatric mice*

Sarcopenia occurs in 18–25-month-old male and female mice [35]. Thus, we treated (*EQ* Old) or not (Untr. Old) 21-month-old C57BL/6 mice with *EQ* (500 mg/kg/day in drinking water) for 3 months, in comparison with untreated adult mice (Adult). Comparable food and water consumption were registered among the experimental groups (Fig. S8A), thus excluding the effects of different intakes on the parameters analyzed. We observed that at the start of the experiment Untr. Old mice showed higher total body weights than adult mice (Fig. 4A). They did not lose body weight during the time of the experiment (Fig. 4A), according to previous data showing that differently from cancer-induced muscle atrophy (*i.e.*, cachexia), age-dependent sarcopenia is not necessarily accompanied by a decrease in body weight [3]. Differently, at the end of the experiment, increased fat weights were measured in Untr. Old *vs* adult mice (Fig. 4B), as expected [3]. *EQ* did not affect either body weight (Fig. 4A) or inguinal and epididymal fat amounts in old animals (Fig. 4B).

Notably, Untr. Old showed reduced *tibialis anterior* (TA), gastrocnemius (GC), and *quadriceps femoris* (QF) muscle weights (up to ~45% reduction) confirming the onset of sarcopenia. In contrast, muscles *EQ* Old had comparable masses to those of Adult mice (Fig. 4C). Moreover, between 21 and 24 months of age, mice experience a drastic drop in force, which was prevented by *EQ* treatment (Fig. 4D), supporting that *EQ* confers protection against age-induced muscle wasting. This was confirmed by the analysis of GC, the muscle most affected by aging [35]. Indeed, GC of Untr. Old mice showed a significant prevalence of atrophic (thin) myofibers (Fig. 4E) and a 31.7% reduction in the average cross-sectional area (CSA) compared with adult mice (Fig. 4F), whereas only an 18.8% reduction of myofiber area was observed in GC of *EQ* Old mice (Fig. 4F). Relating to Untr. Old mice, *EQ* Old mice showed lower percentages of centrally-nucleated myofibers (Fig. S8B,C) and expression of *Myh3* (MyHC3) (Fig. S8D), the embryonic myosin typical of regenerating myofibers [36]. Similar results were obtained in TA muscles (Fig. S9A-C).

3.5. *EQ preserves the expression of MyHC-II in hind-limb muscles of geriatric mice and restrains the metabolic shift to slow-twitch fibers*

The protein levels of MyHC-fast (MyHC-II) were strongly reduced in GC, TA, and QF muscles of Untr. Old mice but not in muscles of *EQ* Old mice compared with adult mice (Fig. 5A and S10A). *EQ* Old GC muscles showed similar expression levels of *Myh4* (MyHC-fast) to those of adult mice (Fig. 5B). In addition, GC muscles of both Untr. Old and *EQ* Old mice contained remarkably higher amounts of MyHC-I (MyHC-slow) protein (Fig. 5A) and increased percentages of slow-twitch fibers (Fig. 5C) compared with adult mice, indicating the occurrence of a shift towards oxidative myofiber type [36]. However, *EQ* reduced the loss of fast fibers in old muscles, translating into a less compromised fast/slow fiber ratio (Fig. 5C).

We found that according to data obtained from recent transcriptome analyses [36], *Foxo6* (Forkhead box O6) and *Foxo1* (Forkhead box O1), which are involved in the maintenance of muscle mass [36], were down-regulated in 27-month-old muscles and maintained at levels similar to adult muscles in *EQ* Old mice (Fig. S10B). Moreover, *EQ* restrained the upregulation of *Il1b*, which may predispose to muscle atrophy [36], in old mice (Fig. S10B). Finally, in agreement with *in vitro* data (Fig. 2A), consumption of *EQ* restrained the activation of STAT3 and NF-κB(p65), as observed in the QF muscles of old mice (Fig. S10C).

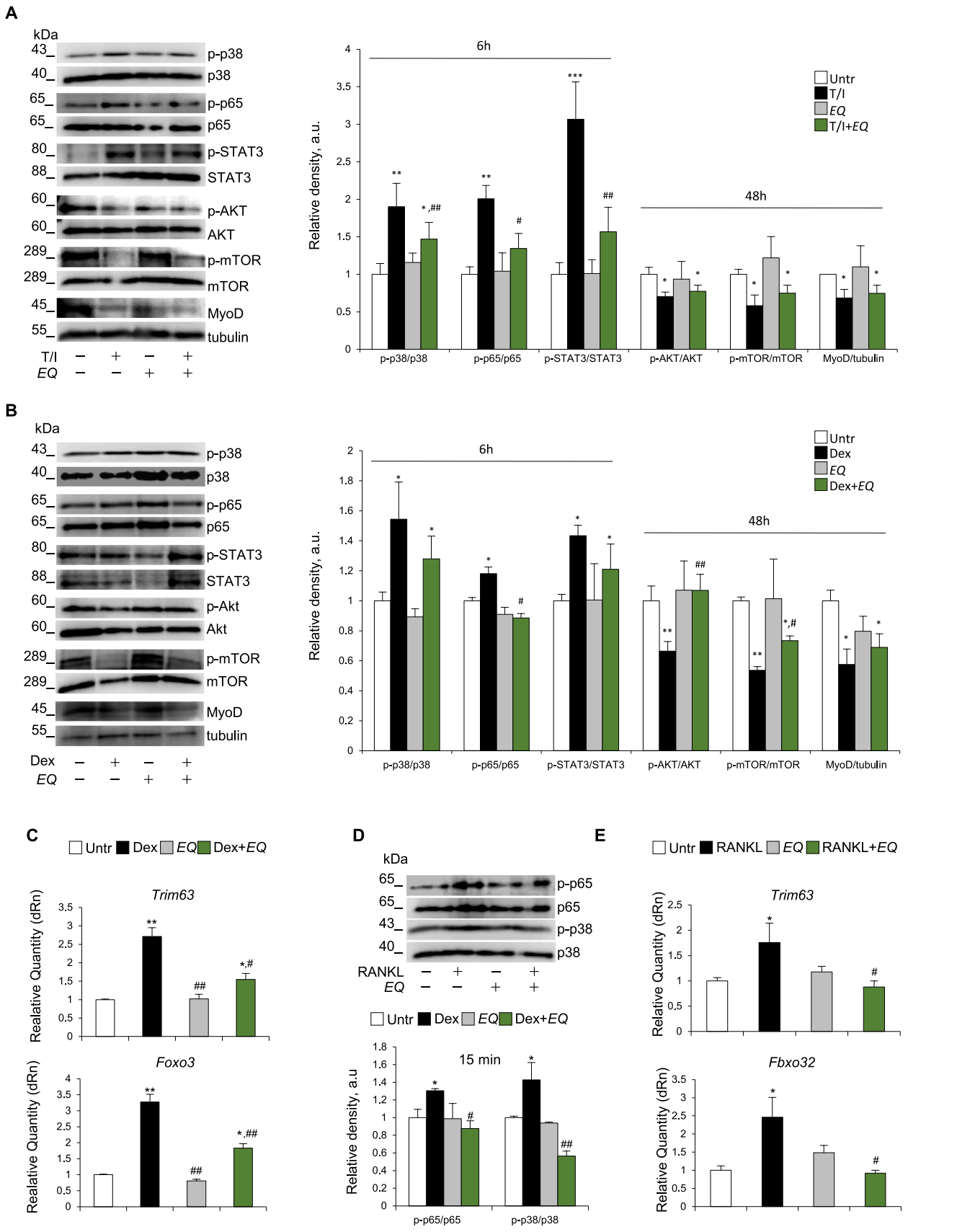

(caption on next page)

Fig. 2. *Equisetum arvense* (*EQ*) extract protects myotubes against atrophy by affecting different pathways depending on the applied stimulus. (A,B) C2C12 myotubes were treated with TNFα (tumor necrosis factor α, 20 ng/mL)/IFNγ (interferon γ, 100 U/mL) (T/I) or dexamethasone (Dex, 1 μM) in the absence or presence of *EQ* (100 μg/mL). After indicated time, total and phosphorylated p38 mitogen-activated protein kinase (MAPK), nuclear factor kappa-light-chain-enhancer of activated B cells (NF-κB)-p65, signal transducer and activator of transcription 3 (STAT3), AKT (protein kinase B), mTOR (mammalian target of rapamycin), MyoD (myoblast determination protein 1) and tubulin levels were analyzed by Western blotting (WB). (C) The expression levels of *Trim63* (Murf-1) and *Foxo3* (Forkhead box O3) were analysed by real-time PCR in myotubes treated with Dex in the absence or presence of *EQ* (100 μg/mL) after 24 h. (D,E) C2C12 myotubes were treated with receptor activator of nuclear factor kappa-B ligand (RANKL, 100 ng/mL) in the absence or presence of *EQ* (100 μg/mL). After 15 min, total and phosphorylated p38 mitogen-activated protein kinase and p65 levels were analyzed by WB (D). See also Fig. S3. The expression levels of the atrogenes, *Trim63* and *Fbxo32* (atrogin-1) were analysed by real-time PCR after 24 h (E). Reported are representative images and the relative densities with respect to tubulin or the total form of phosphorylated proteins (A,B,D). Gene expressions were normalized to *Gapdh* (C,E). Results are means ± standard error of the mean (A,B,D) or ± standard deviation (C,E). Statistical analysis was conducted using the two-tailed *t*-test. * $p<0.05$, ** $p<0.01$ and *** $p<0.001$, significantly different from untreated control; # $p<0.05$ and ## $p<0.01$, significantly different from T/I, Dex, or RANKL.

3.6. EQ counteracts osteopenia in geriatric mice

Despite both male and female C57BL/6 J mice developing osteoporotic features between 18 and 24 months of age [37], gender compartment-specific bone loss and extent of severity have been reported [38]. Thus, given the remarkable effect of *EQ* in counteracting osteoclastogenesis *in vitro* (Fig. 3), we assessed the potential effect of *EQ* in protecting from age-related osteoporosis by performing bone analyses in old female mice, which are characterized by more severe osteoporosis. Female adult mice (n=3) showed a visible tibia metaphyseal zone (METz) formed by a thick layer of chondrocytes (Ch) and characterized at the bottom by the beginning of the trabecular (Tb), which appeared normal and typically dense, uniform, and continuous along the bone, and well-developed cortical zone (Fig. 6A). METz was excluded from the morphometric measurement as it was absent in old ones. The tibiae of female Untr. Old mice (n=3) were characterized by a dramatically altered Tb morphology, which appeared moderately thin with wider spaces and lacking in some areas, in addition to an increase of adipose tissue (AT) (Fig. 6B), indicating a typical osteoporotic histological profile. *EQ* consumption in female old mice (n=3) translated into narrowed separation, improved Tb uniform distribution, and a low presence of AT (Fig. 6C).

The measurement reported in Fig. 6D confirmed a CnAr similar to adult mice in *EQ* Old mice concomitantly with preserved levels of *Col1a1* (collagen type I alpha 1 chain) (Fig. 6F), which is essential in the bone remodeling process [39]. Both parameters were found to decrease enormously in Untr. Old mice (Fig. 6D,F). In line with the recognized susceptibility of trabecular bone to osteopenia, no changes in cortical bone thickness (Cbt) were observed among the different groups (Fig. 6A-C, E), as frequently reported in animal models of osteoporosis [40].

Micro-CT analysis of the tibia (Fig. 7) confirmed Tb decrease in Untr. Old compared with adult mice, morphologically preserved by *EQ* consumption (Fig. 7A). Moreover, Untr. Old mice compared with adult mice revealed a marked decrease in bone volume (BV), bone surface (BS), Tb number (TbN) and percentages of Tb with thickness >0.144 mm (Tb. Th), and an increase in percentages of Tb with thickness <0.144 mm (Fig. 7 B,C). Moreover, a dramatic drop in the connectivity density (Conn.D), another Tb architectural index recently introduced [40], was observed in Untr. Old mice (Fig. 7D). The values of BV and BS in *EQ* Old mice were not significantly different from those of Untr. Old animals and adult mice ($p=0.08$ and $p=0.06$, respectively) (Fig. 7B). Although the *EQ* Old group *vs* adult mice showed a significant decrease in TbN, the percentage of Tb >0.144 mm was doubled *vs* Untr. Old mice (Fig. 7C) and Conn.D were maintained at similar values to adult mice (Fig. 7D). We also evaluated (data not shown) Cbt at the tibia shaft in addition to the trabecular region confirming the absence of significant changes between the samples ($p>0.05$) as reported in histologic and morphometric observations (Fig. 6A-C, E).

3.7. EQ counteracts the age-induced alterations in spleen microarchitecture and inflammatory cytokine profile in geriatric mice

The disruption of splenic microanatomy and the dramatic expansion of immune cells typical of aging contribute to peripheral immunosenescence and inflammaging, common causes of sarcopenia and osteoporosis in the elderly [41]. The spleens of Untr. Old mice were found heavier than those of adult mice (Fig. 8A), and showed hallmarks of active inflammation, including loss of macrophage marginal zone, increased amounts of giant cells, and MAC3-positive macrophages typical of the red pulp infiltrating the white pulp (Fig. 8B-D). In contrast, *EQ* Old mice showed spleen weight and morphology similar to those of adult mice (Fig. 8A,B), MAC3-positive macrophages generally confined to the marginal zone (Fig. 8D), and levels of the pro-inflammatory cytokines *Il1b, Il6, Tnfa* and *Ifng* lower than Untr. Old mice (Fig. 8E).

3.8. Targeted ultra-high performance liquid chromatography-tandem mass spectrometry (UHPLC-MS) analysis of the EQ extract

Our results were obtained using a commercial extract of *EQ* containing 10% silica, which might justify *EQ*'s anti-osteoclastogenic and anti-osteoporotic effects *in vitro* and *in vivo* respectively. However, to explain the unexpected effects of *EQ* on muscle tissue we decided to analyze the most abundant metabolites (mostly of phenolic nature) contained in the plant extract profiling. Thus, based on literature data [42], a targeted MS analysis on the sample was performed by applying the UHPLC-MS. In this way, the fifteen compounds listed in Table 1 were identified. MS/MS spectra are shown in Fig. S11. More in detail, the following species, here distinguished for their structural characteristics, were identified: the iridoid glycoside 8-acetylharpagide; the phenolic acid *trans*-ferulic acid; the chalcone derivative 2′,4′-dihydroxy-4-prenyloxy chalcone; the three flavonoid glycosides isoquercetin, kaempferol-3-*O*-glucoside, and apigenin-4′-*O*-glucoside; the simple non-methylated flavonoids quercetin, kaempferol (or luteolin), and apigenin; the fatty acids monolinolenin, and pinolenic acid; the terpenes myrcene, and dihydroactinidiolide; the simple methylated flavonoids genkwanin, and 7-*O*-methylchrysin.

3.9. In silico target fishing

In the presence of different atrophying stimuli, *EQ* modulated the activation state of specific catabolic and anabolic pathways concluding in the common reduction of phosphorylated/activated NF-κB p65 subunit (Figs. 2 and S5), strongly implicated in age-related diseases including osteoporosis and sarcopenia [43]. To elucidate the role of NF-κB pathway in the mechanism of action of *EQ* and identify potential molecular targets modulated by the compounds highlighted in Table 1, we performed a computational target fishing study. Specifically, we employed the Polypharmacology pLATform prediction (PLATO) tool [44], which is a predictive drug discovery web platform for ligand-based protein target fishing and bioactivity profiling of small molecules. It relies on 2D Tanimoto similarities of the query compounds against a dataset of 632,552 compounds with experimentally measured

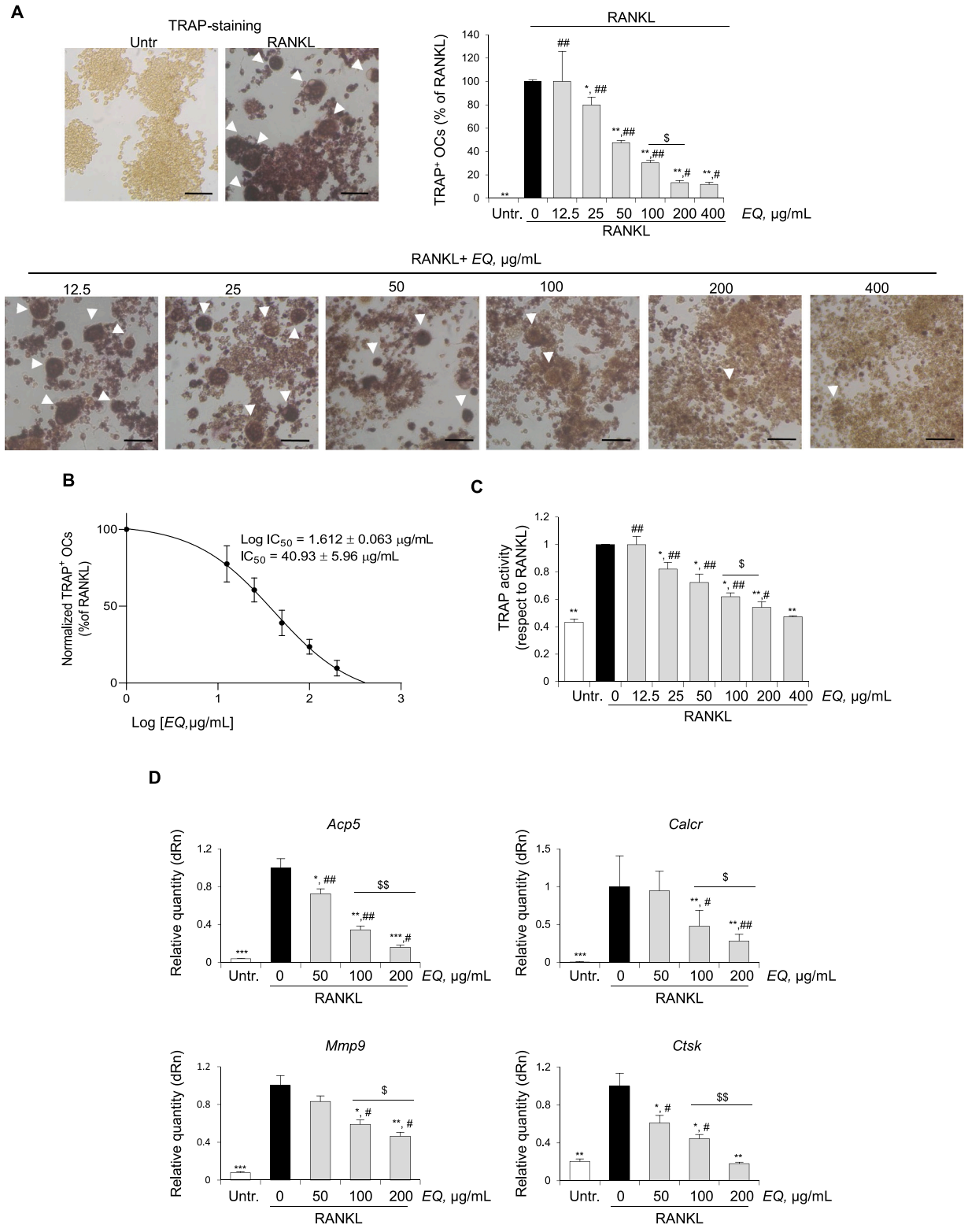

Fig. 3. *Equisetum arvense* (*EQ*) inhibits receptor activator of nuclear factor kappa-B ligand (RANKL)-induced osteoclastogenesis. (A-D) RAW 264.7 cells were treated for 5 days with RANKL in the absence (*black bars*) or presence (*gray bars*) of *EQ* at the indicated doses. Untreated controls (*Untr.*; *white bars*) were also shown. TRAP (tartrate-resistant acid phosphatase) staining was performed and TRAP-positive osteoclasts (OCs; ≥3 nuclei) were counted. Representative images are reported; arrowheads mark OCs (A). A concentration-response curve was obtained to determine the IC_{50} of *EQ* using non-linear regression (B). Supernatants of cells in A were collected, and TRAP activity was measured by TRAP reaction buffer and reported as fold change *vs.* RANKL treatment (assigned value, 1) (*black bar*) (C). See also Fig. S6. Real-time PCR analysis of the OC markers, *Acp5* (acid phosphatase 5, tartrate resistant), *Calcr* (calcitonin receptor), *Mmp9* (matrix metallopeptidase 9), and *Ctsk* (cathepsin K) was performed. Gene expressions were normalized to *Gapdh* and reported as fold change *vs.* RANKL treatment (assigned value, 1) (*black bar*) (D). Six independent experiments were performed. Results are means ± standard error of the mean (A-C) or ± standard deviation (D). Statistical analysis was conducted using the two-tailed *t*-test. * $p< 0.05$, ** $p< 0.01$, and *** $p< 0.001$, significantly different from RANKL; # $p< 0.05$ and ## $p< 0.01$, significantly different from Untr $ $p< 0.05$ and $$ $p< 0.01$, significantly different.

A

Animal	Initial Body weight (g)	Terminal Body weight (g)
Adult	20.5±0.3	23.7±1.4
Untr. Old	25.9±0.1 *	24.9±1.4
EQ Old	26.7±0.3 *	24.4±1.1

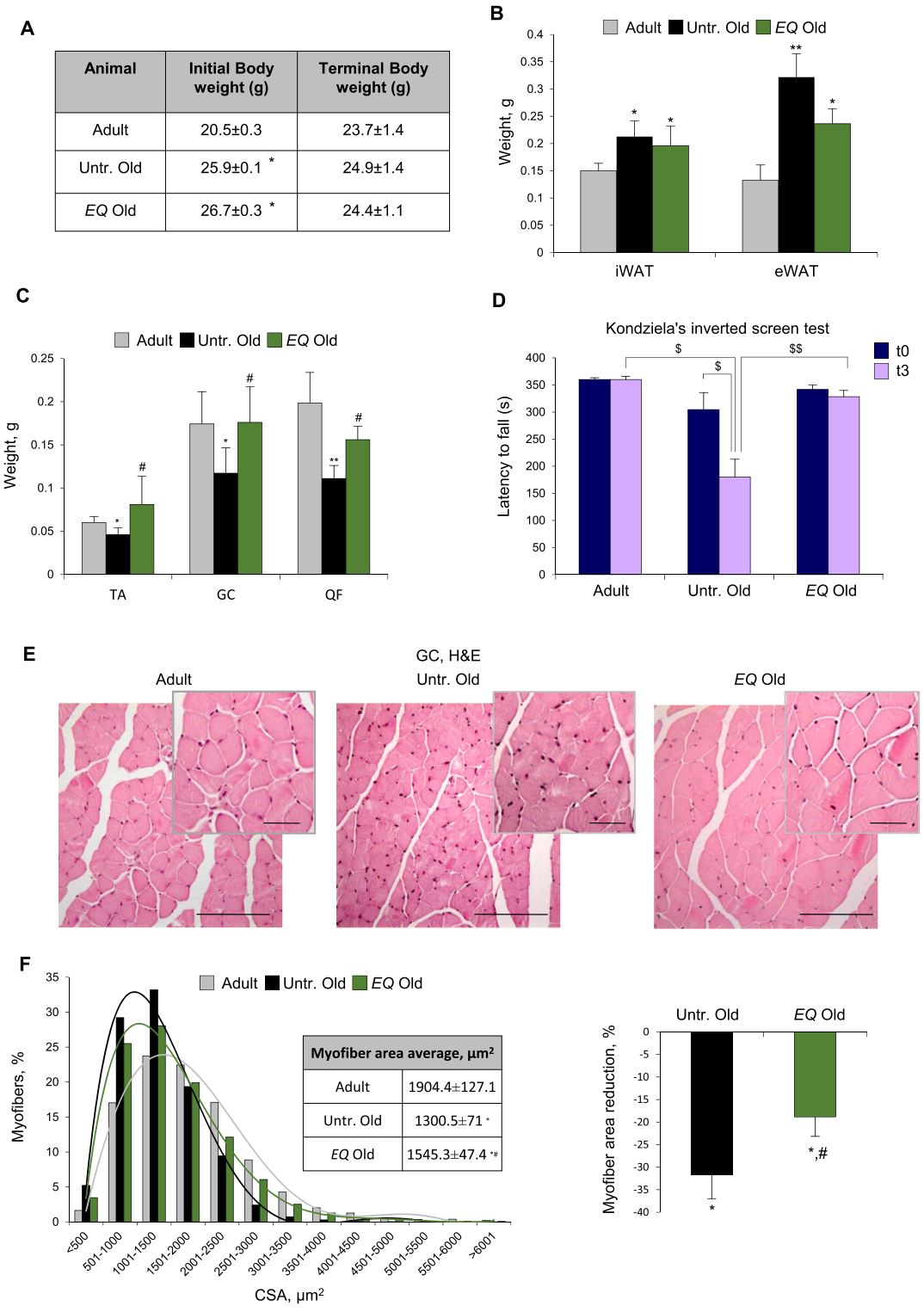

Fig. 4. *Equisetum arvense* (*EQ*) extract counteracts the loss of muscle mass and performance in geriatric mice. (A-F) Pre-geriatric C57BL/6 mice were administered with (*EQ* Old) or not (Untr. Old) *EQ* (500 mg/Kg/die) melted directly in the water for 3 months. Six-month-old C57BL/6 mice were used as control (adult). Body weights were measured at the beginning and the end of experimentation and the average for each group of animals is reported (A). After sacrifice, inguinal (iWAT) and epididymal (eWAT) white adipose tissue (B), and *Tibialis anterior* (TA), *Gastrocnemius* (GC), and *Quadriceps femoris* (QF) muscles were weighed (C). Reported are the means of time latencies to fall in Kondziela's inverted screen test performed at the beginning (t0) and the end (t3) of the experiment (D). GC muscles were formalin-fixed and paraffin-embedded, and hematoxylin/eosin (H&E) staining was performed. Representative images and high-magnification insets are reported (E). Reported data are the average percentages of GC myofiber cross-sectional area (CSA) in each diameter range measured by *Image J* software and the average myofiber areas (μm^2) for the different animal groups. The percentage changes of *Gastrocnemius* (GC) myofiber areas *vs* adult mice are also reported (F). Results are means ± standard error of the mean. Statistical analysis was conducted using the two-tailed *t*-test. * $p<0.05$ and ** $p<0.01$, significantly different from adult; # $p<0.05$, significantly different from Untr. Old. $ $p<0.05$ and $$ $p<0.01$ significantly different. Scale bars (E), 200 µm.

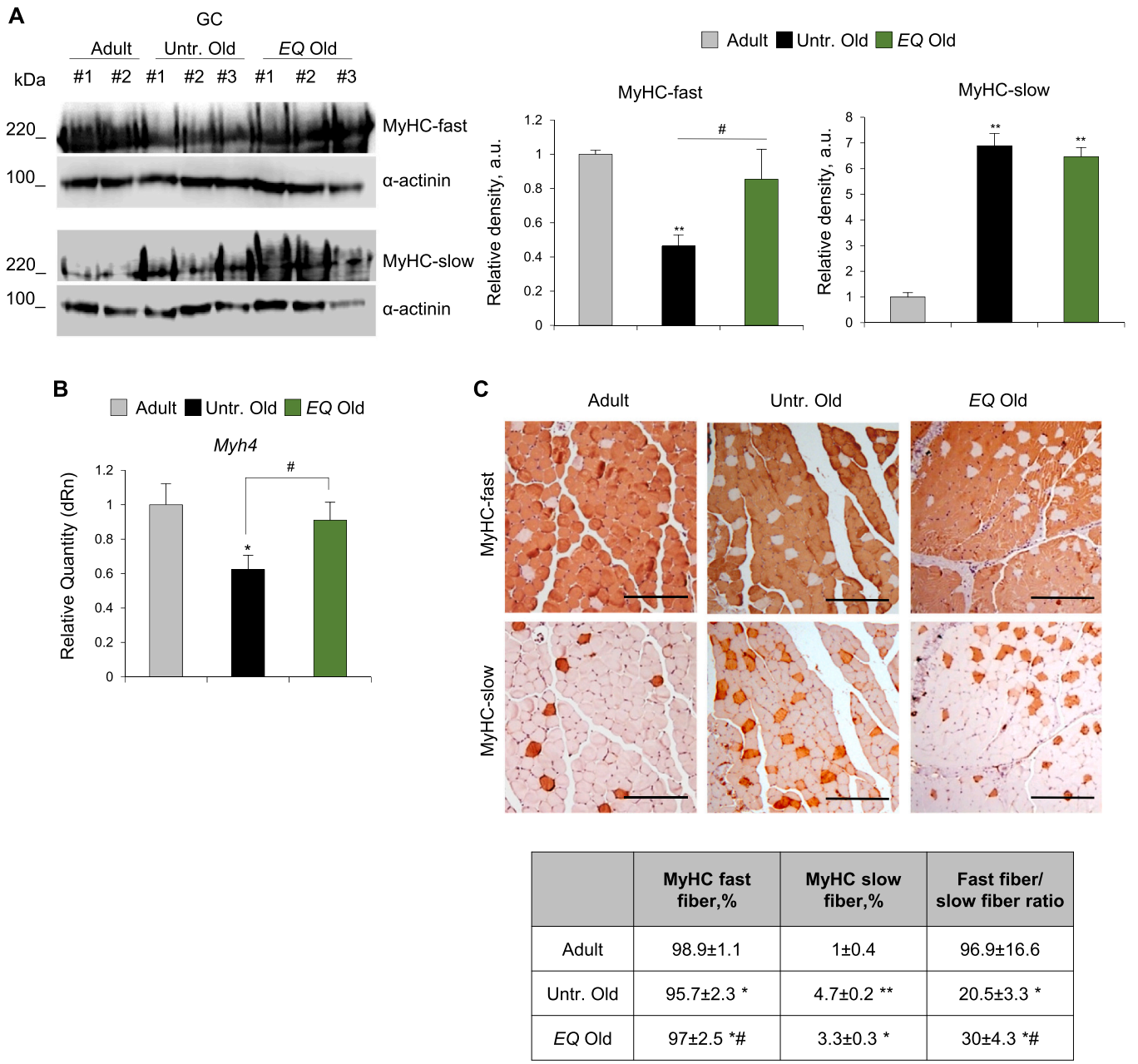

	MyHC fast fiber,%	MyHC slow fiber,%	Fast fiber/ slow fiber ratio
Adult	98.9±1.1	1±0.4	96.9±16.6
Untr. Old	95.7±2.3 *	4.7±0.2 **	20.5±3.3 *
EQ Old	97±2.5 *#	3.3±0.3 *	30±4.3 *#

Fig. 5. *Equisetum arvense* (*EQ*) extract preserves the expression of fast myosin heavy chain (MyHC) isoform in hind-limb muscles of geriatric mice. (A-C) GC muscles of adult and pre-geriatric C57BL/6 mice treated (*EQ* Old) or not (Untr. Old) with *EQ* were excised after the sacrifice and processed for different analyses. The expression of fast and slow MyHC isoforms was evaluated by Western blotting. Reported are representative images and relative densities with respect to α-actinin (A). *Myh4* (*Myosin light chain 4*), the gene encoding for the fast MyHC-IIb isoform, was analyzed by real-time PCR. Gene expressions were normalized to *Gapdh* (B). The expression of slow and fast MyHC isoforms was evaluated by immunohistochemistry. The table reported the average percentage and ratio of fast and slow myofibers for the different animal groups (C). Reported are representative images (A,C). Results are means ± standard error of the mean. Statistical analysis was conducted using the two-tailed *t*-test. $^{*}p<0.05$ and $^{**}p<0.01$, significantly different from adult; $^{\#}p<0.05$, significantly different from Untr. Old.

bioactivity data for 6047 protein targets sourced from ChEMBL release 32 [45]. Each compound listed in Table 1 underwent thorough analysis using the PLATO platform, which suggested several potential targets for each query molecule. To refine the selection, the protein targets were subsequently subjected to stringent filtration criteria: i) minimum score threshold (≥5) and reliability assessment (reliable: yes) to ensure that only the most pertinent macromolecules were retained for further investigation; and ii) involvement in modulating the activation status of NF-kB p65.

From the computational target fishing approach, five proteins involved in NF-kB p65 activity emerged as potential targets of the investigated compounds (Table 2). In particular, eight out of fifteen compounds i.e., isoquercetin, quercetin, kaempferol-3-*O*-glucoside, luteolin, apigenin-4'-*O*-glucoside, apigenin, genkwanin and 7-*O*-methylchrysin could potentially target IKKB, the primary enzyme responsible for the phosphorylation and subsequent degradation of the NF-kB inhibitor IκB that directly binds p65 subunit. The degradation of IκB allows p65 to be phosphorylated and enter allowing its phosphorylation and entry into the nucleus to regulate gene transcription [46].

We also found the following proteins as potential targets: i) PPARγ, which physically interacts as an E3 ubiquitin ligase with p65 to induce its ubiquitination and degradation [47]; ii) adenosine receptors, which attenuate NF-κB p65 phosphorylation [48]; iii) STAT3, which physiologically binds p65 amplifying the transcription of inflammatory genes

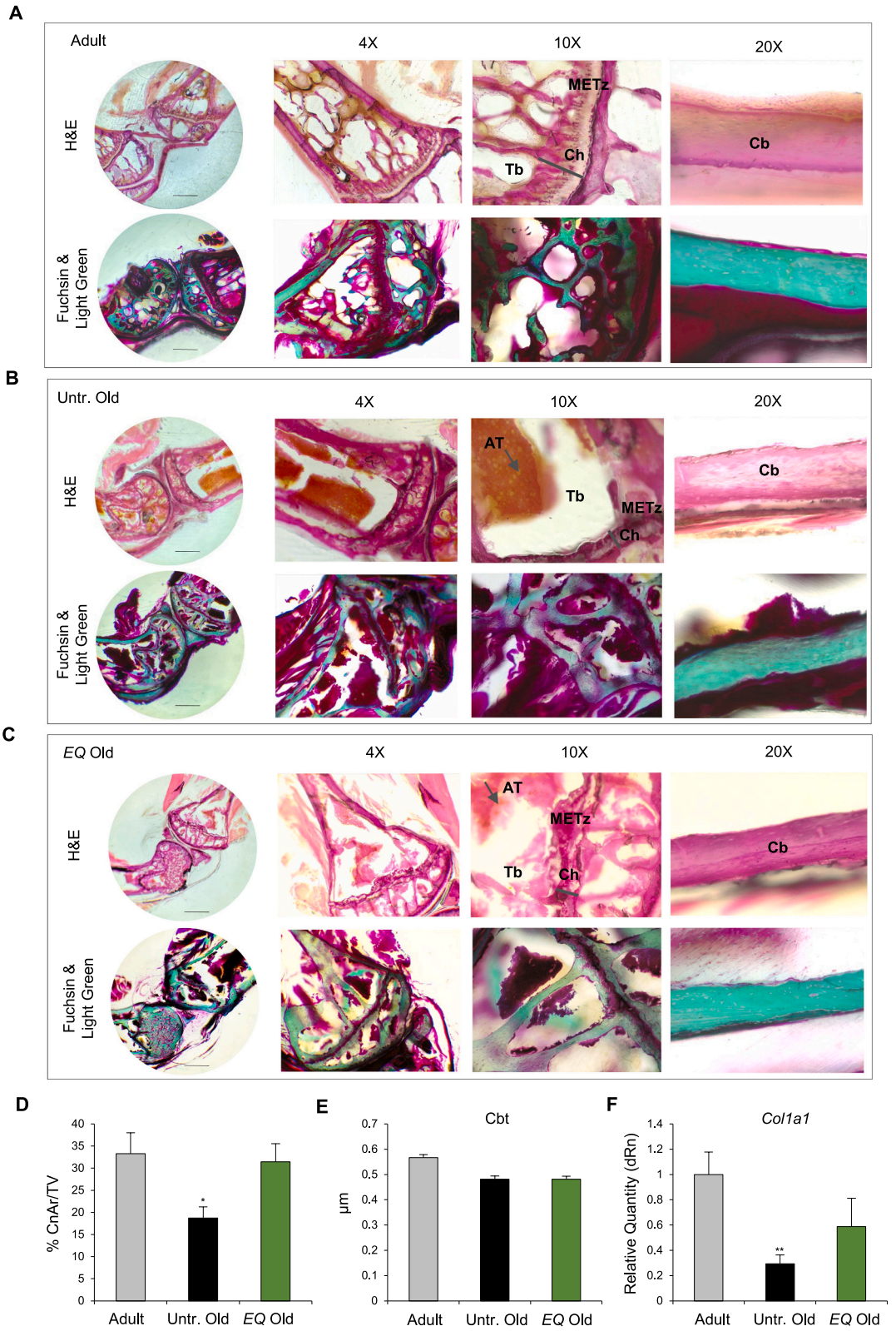

Fig. 6. *Equisetum arvense* (*EQ*) extract restrains the aging-related histological change of the bone. (A-F) Left femur and tibia from adult and pre-geriatric C57BL/6 mice treated (*EQ* Old) or not (Untr. Old) with *EQ* were excised after the sacrifice and processed no disarticulated for different analyses. Representative images at different magnifications were obtained after hematoxylin/eosin (H&E) or Fuchsin/Light green staining. AT, adipose tissue; Cb, cortical bone zone; Ch, chondrocytes; METz, metaphyseal zone; Tb, trabeculae. Scale bars, 200 nm (A-C). Morphometric measurements of cancellous bone area (CnAr)/tibia volume (TV) and cortical bone thickness (Cbt) (D,E). Expression of *Col1a1* (collagen type I alpha 1 chain protein) was analyzed by real-time PCR. Gene expression was normalized to *Gapdh* (F). Results are means ± standard error of the mean. Statistical comparison was performed with One-way ANOVA, Tukey's Test (A-E) or two-tailed *t*-test (F). * $p<0.05$ and ** $p<0.01$, significantly different from adult.

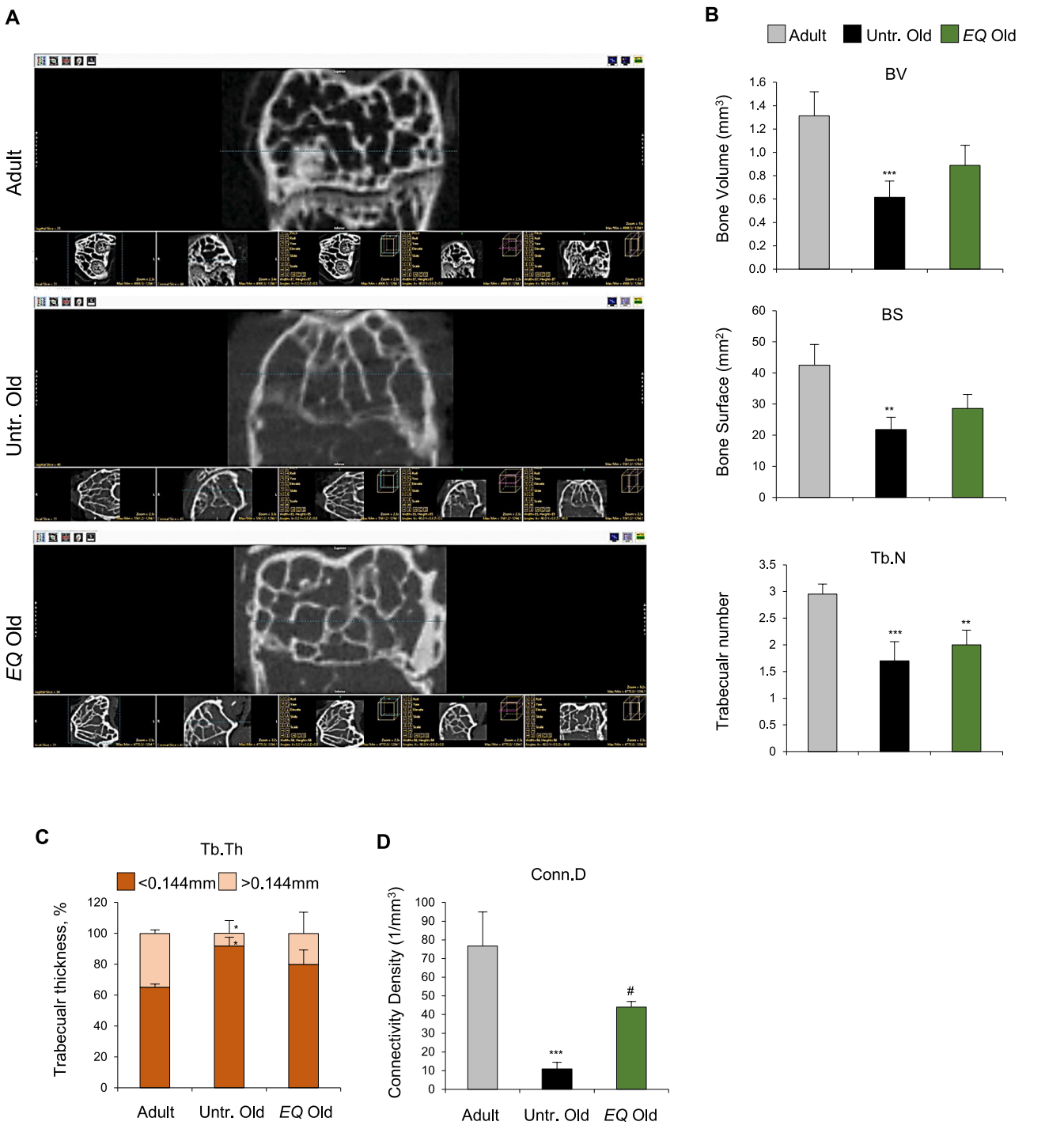

Fig. 7. Evaluation of *Equisetum arvense* (*EQ*) consumption in bone microarchitecture status by micro-CT. (A-D) The right tibia from adult and pre-geriatric C57BL/6 mice treated (*EQ* Old) or not (Untr. Old) with *EQ* were excised after the sacrifice and processed for different analyses. In the main panels, representative longitudinal Micro-CT images of the tibia in 2D dimension are shown. The other images show sagittal, axial and coronal sections (from left to right, respectively) (A). Graphs reported BV (Bone Volume of the segmented region in mm^3), BS (Bone Surface of the segmented region in mm^2), Tb. N (Trabecular number, measured as the average number of Tb/1/mm length), Tb.Th (Trabecular thickness, assessed in mm using direct 3D methods and reported as percentages), and Conn. D (Connectivity density of segmented region in $1/mm^3$) (B-D). Results are means ± standard error of the mean. Statistical comparison was performed with One-way ANOVA, Tukey's Test (B) or two-tailed *t*-test (C,D). * $p<0.05$, ** $p<0.01$, and *** $p<0.001$, significantly different from adult. # $p<0.05$, significantly different from Untr. Old.

[49] and iv) RSK1, which phosphorylates IκB contributing to the persistent activation of NF-κB [50]. These data strongly support the involvement of NF-κB pathway in the *EQ*'s anti-atrophic effects, and suggest IKKB as a major target of the active compounds tested.

Furthermore, among the predicted targets, IKKB emerges as the foremost candidate warranting further investigation. Interestingly, previous computational studies identified the compound quercetin as a possible ligand of the specific ATP-binding pocket of IKKB [51], thus attenuating LPS-dependent NF-κB activation [52]. Since we observed that *EQ* exerted similar biological effects of quercetin (Figs. 2 and S5), we performed molecular docking experiments to investigate the potential intermolecular interactions between the eight molecules in Table 2

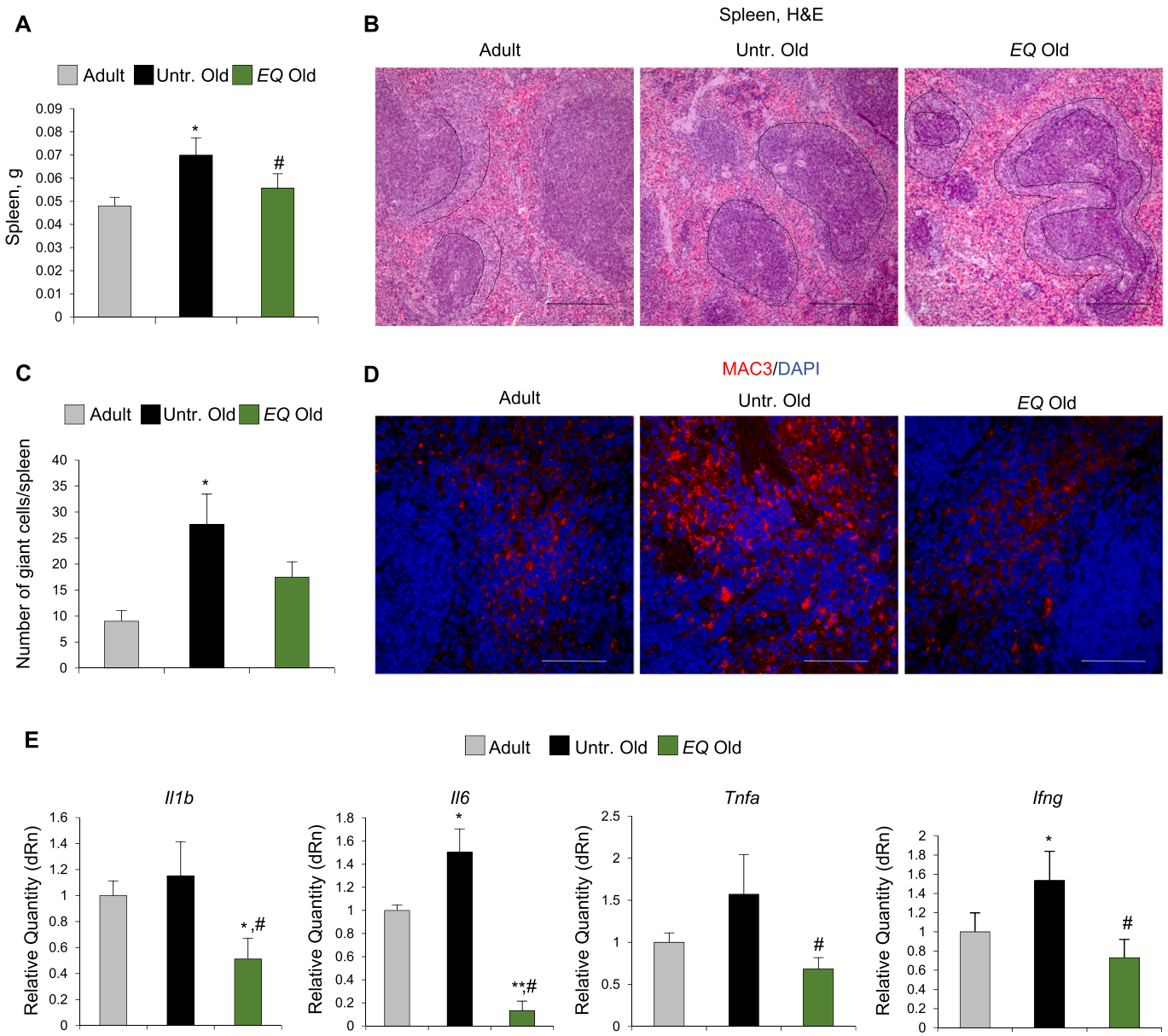

Fig. 8. *Equisetum arvense* (*EQ*) extract maintains spleen morphology and counteracts age-dependent increase of pro-inflammatory cytokines. (A-E) Spleens of adult C57BL/6 mice, and geriatric mice treated (*EQ* Old) or not (Untr. Old) with *EQ* were weighed *post-mortem* (A), and formalin-fixed and paraffin-embedded before hematoxylin/eosin (H&E) staining. Dashed lines define the marginal zone between white and red pulps (B). The number of giant cells was reported (C). Expression of the activated macrophage marker, MAC3 was analysed in spleen sections by immunofluorescence. 4′, 6-diamidino-2-phenylindole (DAPI; *blue*) was used to stain nuclei (D). The levels of the pro-inflammatory cytokines *Il1b* (interleukin 1β), *Il6* (interleukin 6), *Ifng* (interferon-γ), and *Tnfa* (tumor necrosis factor α), were evaluated by real-time PCR. Gene expressions were normalized to *Gapdh* (E). Reported are representative images (B,D). Results are means ± standard error of the mean. * $p<0.05$ and ** $p<0.01$, significantly different from adult; # $p<0.05$, significantly different from Untr. Old. Scale bars (B,D), 250 μm.

and the protein kinase IKKB. All the compounds demonstrated a favorable predicted binding affinity (docking scores ranging from −7.21 to −9.77 Kcal/mol) as well as the ability to establish favorable contacts with the pocket residues. Specifically, the eight compounds showed common interactions involving Leu21, Val29, Glu97, Tyr98 and Cys99 (Table 3). The highest predicted affinity was observed for genkwanin (docking score of −9.77 Kcal/mol). In its predicted binding mode, this small molecule established i) two hydrogen bonds with the backbone of the hinge residues Glu97 and Cys99 (Fig. 9), ii) an additional hydrogen-bond with Lys44, and iii) favorable contacts with Leu21, Val29, Ala42, Met96, Glu97, and Gly102 (Table 3).

The observations emerged from the *in silico* analysis pave the way for further future studies to validate the putative molecular targets modulated by the single *EQ* active compounds.

4. Discussion

Sarcopenia and osteoporosis are associated with unhealthy aging and coexist in osteosarcopenia (OS), the most prevalent musculoskeletal syndrome in the elderly, favoring the loss of function in daily activities, co-morbidities, fragility, falls, hospitalizations, and mortality [1–3]. Efficacious treatments simultaneously affecting muscle and bone are still missing although enormously urgent due to the sharp increase in the aging population. Herbal extracts have recently aroused interest in human health research also in osteoporosis or sarcopenia conditions [53], and natural bioactive compounds such as resveratrol or epigallocatechin-3-gallate in combination with physical exercise have been partially validated in sarcopenic women [54,55].

Here, for the first time, we deeply investigated the effects of *EQ* on

Table 1
Results of the targeted MS and MS^2 analysis. Compounds are listed according to their retention time and recorded using the applied method. In bold, the fragment with the highest intensity. The relatively low score is due mainly to poor signal-to-noise ratio (a). Despite the coelution of the pairs Isoquercetin/Quercetin and Kaempferol-3-*O*-glucoside/Kaempferol (or Luteolin), the appraisal of the chemical identity was however possible (b).

Cpd	RT	*m/z*	MS^2 fragment[a]	Formula	Exp Mass	Calc Mass	Score	Error (in ppm)	Possible Candidate
1	0.715	424.1777 $[M+NH_4]^+$	409.1570, 348.1471, 275.0944, 239.0682, **180.0603.**	$C_{17}H_{26}O_{11}$	406.1453	406.1475	58.33[b]	-5.49	8-Acetylharpagide
2	4.35	195.0637		$C_{10}H_{10}O_4$	194.0565	194.0579	67.81	-7.31	Ferulic Acid
3	4.466	342.17 $[M+NH_4]^+$	297.1119, **265.0854**, 222.0664, 191.0838, 85.0590.	$C_{20}H_{20}O_4$	324.1363	324.1362	79.63[b]	0.49	2',4'-dihydroxy-4- prenyloxy chalcone
4	4.914	465.1034	**303.0860,** 285.0762, 257.0803, 209.0444, 167.0329.	$C_{21}H_{20}O_{12}$	464.0955	464.0955	99.56	-0.03	Isoquercetin[c]
5	4.914	303.0496	286.0466, 231.0645, **151.0400**, 77.0399, 55.0532.	$C_{15}H_{10}O_7$	302.0424	302.0427	99.14	-0.96	Quercetin[c]
6	5.13	449.1070	393.1851, **287.0553,** 224.0925, 153.0174, 97.0261.	$C_{21}H_{20}O_{11}$	448.1010	448.1006	98.59	0.92	Kaempferol-3-*O*-glucoside[c]
7	5.13	287.0552		$C_{15}H_{10}O_6$	286.0479	286.0477	85.75	0.7	Kaempferol (or Luteolin)[c]
8	5.246	433.1127	**271.0611,** 193.0871, 137.0960, 111.0794, 91.0536.	$C_{21}H_{20}O_{10}$	432.1059	432.1056	83.94	0.51	Apigenin-4'-*O*-glucoside
9	7.354	271.0603	242.0571, 166.0593, **153.0175,** 119.0495, 57.0702.	$C_{15}H_{10}O_5$	270.053	270.0528	96.33	0.55	Apigenin
10	7.586	370.2942 $[M+NH_4]^+$		$C_{21}H_{36}O_4$	352.2604	352.2614	95.18	-2.69	Monolinolenin
11	7.752	137.1322		$C_{10}H_{16}$	136.1252	136.1252	90.91	-0.1	Myrcene
12	8.283	203.1048 $[M+Na]^+$		$C_{11}H_{16}O_2$	180.1157	180.115	73.57[b]	3.65	Dihydroactinidiolide
13	8.814	285.0756	270.0520, **242.0570,** 197.0602, 167.0340, 124.0154.	$C_{16}H_{12}O_5$	284.068	284.0685	97.92	-1.57	Genkwanin
14	9.528	269.0817		$C_{16}H_{12}O_4$	268.0742	268.0736	81.34	2.56	7-*O*-Methylchrysin
15	9.644	279.2311		$C_{18}H_{30}O_2$	278.2244	278.2246	82.14	-0.69	Pinolenic acid

Table 2
The five potential targets and related scores (when available) computed for each examined compound. The CHEMBL target ID provided by the PLATO tool is also reported for each target.

Compound	NR1C3 (CHEMBL235)	ADORA1 (CHEMBL226)	IKKB (CHEMBL1991)	STAT3 (CHEMBL4026)	ISPK1 (CHEMBL2345)
8-Acetylharpagide				7.01	
Ferulic Acid				7.49	
2',4'-dihydroxy-4- prenyloxy chalcone					
Isoquercetin[c]			9.47		11.63
Quercetin[c]		7.98	8.83		
Kaempferol-3-*O*-glucoside[c]			7.99		12.12
Kaempferol (or Luteolin)[c]	11.69	12.55	8.78	9.19	
Apigenin-4'-*O*-glucoside			9.52		10.36
Apigenin	13	13	8.97	10.1	
Monolinolenin					
Myrcene					
Dihydroactinidiolide					
Genkwanin	11.75	7.72	7.02	6.88	
7-*O*-Methylchrysin	11.16	11.71	7.71		
Pinolenic acid	12.39				

both skeletal muscle and bone homeostasis *in vitro* and its translational potential as a treatment for OS *in vivo*. *EQ* is traditionally considered a treatment to prevent osteoporosis [8], and a beneficial effect on skeletal muscle could be seen as an indirect consequence of bone-muscle cross-talk. However, our data demonstrate that *EQ* directly affects muscle cells, both myoblasts and differentiated myotubes, where it has pro-myogenic and anti-atrophic activity, respectively. Indeed, *EQ* accelerates myoblast terminal differentiation and fusion into myotubes likely by activating the pro-myogenic p38 MAPK-myogenin axis. *EQ* maintains the myogenic potential of muscle precursor cells in the presence of atrophying stimuli, preserving myotube growth by adding nuclei derived from non-fused myoblasts. Notably, *EQ* does not rely on an intrinsic hypertrophic effect, as it does not affect myotube trophism in physiological conditions. More importantly, *EQ* counteracts the reduction in myotube diameter and MyHC-II expression under atrophying stimuli mimicking low-grade chronic systemic inflammation, treatment with steroids, or exposure to altered levels of osteokines, *i.e.*, the leading causes of muscle protein degradation in sarcopenia [3,6]. Indeed, in the presence of T/I, *EQ* reduces the levels of catabolic p38 MAPK and the transcription factor STAT3, known to complex NF-kB thus inhibiting MyoD-induced MyHC-II synthesis [25]. Unexpectedly, *EQ* does not affect MyoD expression, suggesting that another downstream effector of STAT3, *e.g.* inducible nitric oxide synthase (iNOS), is used to protect against T/I-induced atrophy [29]. In Dex-dependent atrophy, *EQ* reduces key muscle atrogenes and sustains protein synthesis, by maintaining the physiological activation state of NF-kB and Akt-mTOR axis, respectively. The reduced NF-kB activation might also prevent the decrease of the anabolic Akt-mTOR pathway, as reported in fasting with high levels of glucocorticoids [56]. Thus, in all the atrophying conditions tested, *EQ* maintains a physiological activation state of the catabolic and anabolic pathways specifically affected in myotubes, by inhibiting NF-κB as a common mechanism. The *in silico* target fishing approach confirms that the pharmacological effect of the analyzed *EQ* active compounds likely consists in modulating the activity of proteins

Table 3
Docking scores and number of contacts that each investigated compound established with the IKKB pocket residues in its predicted binding mode.

	Genkwanin	Kaempferol-3-*O*-glucoside[c]	Apigenin	7-*O*-Methylchrysin	Quercetin	Kaempferol (or Luteolin)	Isoquercetin	Apigenin-4'-*O*-glucoside
Docking score (Kcal/mol)	-9.77	-9.52	-9.45	-8.94	-8.93	-8.85	-8.76	-7.21
Glu19								3
Arg20								5
Leu21	5	11	3	6	6	6	8	13
Gly22		3					3	
Thr23							1	
Val29	4	3	4	3	3	3	6	2
Ala42	3		3	2	3	3		4
Lys44	4	3	4	1	3	3	4	
Glu61					2	1	4	
Met96	2		2	2	5	3	3	2
Glu97	3	3	3	1	1	1	1	4
Tyr98	2	2	1	2	1	1	1	2
Cys99	4	4	3	5	4	4	3	4
Gly102	2		2	2	1	1	1	3
Asp103		6		2	1	2	5	7
Lys106								1

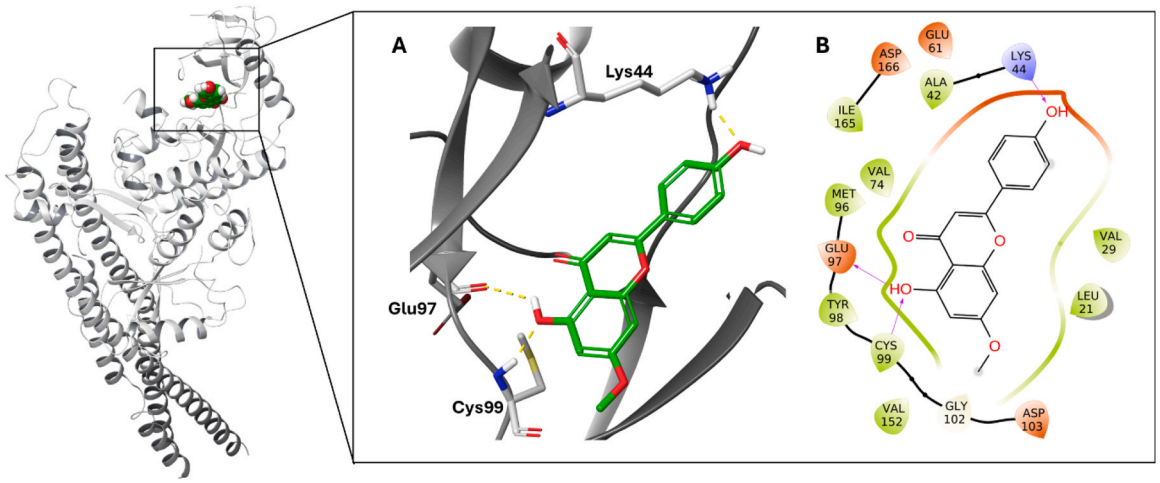

Fig. 9. Molecular docking studies of genkwanin on protein kinase IKKB. 3D (A) and 2D (B) representation of the predicted binding mode of genkwanin to IKKB.

participating in the NF-κB signaling, including STAT3 and IKKB, which emerges as the foremost candidate. The possible involvement of PPARγ, adenosine receptors, and S6K1 in the mechanism used by *EQ* in exerting its beneficial effects deserves further investigation. Interestingly, PPARγ [57] and S6K1 [58] have a role in skeletal muscle metabolism, and the regulation of protein quality and muscle force, respectively.

In old mice, *EQ* consumption delays the appearance of sarcopenia translating into strong resistance against the loss of muscle protein and mass (weight and cross-sectional area, respectively) using mechanisms similar to those observed *in vitro*. *EQ* specifically preserves the physiological amount of MyHC-II, which is expressed in fast-twitch glycolytic myofibers and responsible for skeletal muscle power and speed of movement and is preferentially degraded in sarcopenia [59], translating into unchanged muscle functionality in *EQ* Old *vs* adult mice. Although *EQ* does not inhibit the age-dependent shift towards slow-twitch oxidative myofibers, it partially contrasts the fast/slow fiber ratio reduction in old muscles, likely acting on motor unit composition, mainly associated with metabolic myofiber changes [38]. Moreover, *EQ* Old mice showed lower compensatory muscle regeneration process activation, *i.e.*, reduced number of centrally nucleated myofibers and *Myh3* levels *vs* Untr. Old mice, suggesting less age-related stress accumulation and impaired repair capacity [36].

EQ strongly counteracts the RANKL-dependent OC differentiation and functionality, as evidenced by the reduced number of TRAP-positive cells, big F-actin rings indispensable for OC adhesion to the bone matrix and bone resorption, the appearance of molecular markers of mature OCs involved in extracellular matrix proteolysis, and reduced OC activity mediator, TRAP [11,13,14]. As revealed by viability assay, the absence of toxic effects of *EQ* in RANKL-derived OCs, strengthens the direct anti-osteoclastic effects of *EQ*. Together with the known ability of *EQ* to stimulate OBs [12,14,60], our data on OCs, strongly suggest that *EQ* might counteract the age-dependent imbalance of bone turnover. Based on our target fishing results, further investigation on adenosine receptors, which are involved in bone turnover [61], is encouraged since these receptors are likely involved in the *EQ*-dependent suppression of NF-κB activity and in subduing RANKL-induced OC differentiation.

Notably, the effects on OCs observed *in vitro* translated into the beneficial effect of *EQ* administration against age-induced osteoporosis *in vivo* in old female mice. Collagen is an osteogenic biomarker with an essential role in bone remodeling, and decreases with aging impairing the mechanical properties of bone [62]. Indeed, *Col1a1* in Untr Old mice was significantly lower than in adult mice, and *EQ* increased its mRNA expression indicating the presence of more active OBs. Micro-CT scanning of the tibia of 24-month-old female mice showed that *EQ* diet supplement inhibits the reduction of bone volume and surface induced by aging, likely through repression of OC formation and activity as suggested by *in vitro* data. The thinning of trabeculae was also preserved by *EQ* treatment in old mice. In particular, trabecular connectivity is a

fundamental property of 3D network, vital for maintaining bone volume and subsequent strength. Bone volume decrease corresponds to connectivity decline, possibly due to loss of small-diameter interconnecting trabeculae [40] as found in bones of Untr Old mice. *EQ* Old mice keep this parameter closer to adult mice confirming to slow down the osteopenic trabecular bone modification typically associated with aging. Data obtained in old mice suggest that *EQ* supplementation is sufficient to preserve a good bone microarchitecture and metabolism in the elderly. However, some parameters investigated were not significantly affected by *EQ* consumption, possibly due to the low number of old female mice. Therefore, further studies designed explicitly on OS treatment in a larger number of geriatric female mice are needed.

Data showing that *EQ* contrasts RANKL-dependent atrophy and osteoclastogenesis are particularly relevant for OS, suggesting that *EQ* might prevent osteoporosis and sarcopenia reducing the excessive RANKL activities in old mice. We also elucidated that RANKL, a critical factor in the muscle-bone crosstalk, induces atrophy mainly activating NF-kB, as demonstrated by its inability to reduce myotube diameter and atrogenes upregulation in the presence of BAY11–7082. The unaltered levels of Akt-mTOR suggest that RANKL does not interfere with muscle protein synthesis.

Thanks to its high content in silica, *EQ* is known to induce bone regeneration and inhibit osteoclastogenesis *in vitro* [60,63], and enhance bone mineralization and formation in ovariectomized rats [33]. In addition to silica, secondary metabolites in our *EQ* extract represent a surprisingly potent cocktail in limiting osteoclastogenesis *in vitro* and regulating bone remodeling *in vivo* based on previously published data. Flavonoids contained in *EQ* extract might be responsible for its effects on osteoporotic bone, considering that isoflavonoids and prenyl flavonoids maintain bone density and strength in menopausal women [64,65] and in ovariectomized rats [66], respectively [67]. In particular: i) quercetin targets both OC progenitors and mature OC suppressing bone resorption by inhibiting differentiation and actin ring formation in mature osteoclasts [68]; ii) kaempferol with anti-inflammatory and anti-oxidative properties showed anti-osteoporotic effects in different experimental models of osteoporosis such glucocorticoid-treated and ovariectomized (OVX) mice as well as bone fracture models by interacting with its estrogenic receptor and modulating BMP-2, NF-κB, MAPK, and mTOR signaling pathways [69]; iii) apigenin significantly suppressed trabecular bone loss, and increased the mineral content and density of the trabecular bone without affecting cortical bone loss in OVX animals [70,71]. Moreover, ferulic acid suppresses osteoclast fusion, differentiation and bone erosion via the inhibition of RANKL dependent NF-κB signaling pathway *in vitro* [72,73] and protects neonatal rats against glucocorticoid-induced osteoporosis by activating SIRT1 and NF-κB [74].

Interestingly, low doses of glycosides kaempferol-3-O-glucoside (GKA) strongly suppressed osteoclastogenesis induced by RANKL and the bone resorption activities by inhibiting the p38 MAPK pathway and showed a therapeutic effect on the osteolytic bone loss induced by LPS and OVX *in vivo* significantly improving bone loss indexes, including BV/TV, Tb.Th, Tb.N, and Conn.D, suggesting that GKA content might be mainly responsible for reducing the total amount of osteoclasts and density of osteoclasts per bone surface in old mice treated with *EQ* [75].

The content of simple flavonoids in our extracts might also explain EQ's notable effects on the preservation of muscle trophism under multiple atrophying conditions [76]. In C2C12 myotubes, quercetin suppressed TNF- and Dex-induced myotube atrophy by reducing the ubiquitin ligases and by regulating mitochondrial membrane potential and reducing ROS production, respectively [77,78]. Moreover, quercetin treatment has been extensively associated with preventing muscle atrophy in different experimental animal models *i.e.*, obesity- or Dex-induced muscle atrophy, cancer-associated cachexia, suspension- or denervation-induced muscle atrophy. The quercetin-dependent reduction of muscle mass loss in atrophic conditions is due to different mechanisms as reported for our *EQ* extract including the attenuation of protein degradation through MuRF-1 and Atrogin-1 downregulation by phosphorylation of Akt and the modulation of inflammatory cytokine release and their downstream signaling pathways [79–81]. Interestingly, long-term (24 weeks) oral treatment with quercetin glycoside effectively improved motor performance and increased muscle (quadratus femoris, gastrocnemius, tibialis anterior, and soleus) mass during the early stages of aging [82]. Similarly, apigenin, highlighted for its anti-atrophic effect *in vitro* and *in vivo,* prevented aging-induced loss of hind-limb muscle mass, and increased the muscle fiber size in aged mice by reducing oxidative stress [76,83] and enhancing muscle function. The potential role of apigenin in preventing age-related sarcopenia has been attributed to the promotion of myosin expression and its pro-myogenic activity in C2C12 cells [84]. Thus, apigenin content might be responsible for the pro-myogenic effect of *EQ* in physiological and atrophying conditions. Additionally, in denervated mice, apigenin attenuated the loss of muscle mass by specific upregulation of fast MyHC [85].

Interestingly, the administration of ferulic acid promoted fast glycolytic and slow oxidative muscle growth in Dex-induced myopathic rats by downregulating myostatin and oxidative stress [86]. In a zebrafish model, ferulic acid administration for 30 days caused the hypertrophic growth of fast-type myofibers by promoting protein synthesis and increasing the expression of transcription factors myogenin and MyoD [87].

According to the molecular docking results, genkwanin emerges as the virtual optimal antagonist among those screened of the IKKB ATP binding site, resulting in sustained cytoplasmic retention of NF-κB and reduction of muscle atrophy in the presence of different atrophying stimuli. Previous results showed that genkwanin exerts an anti-rheumatoid arthritis effect by targeting proteins of NF-κB pathway, including IKKs, thus reducing inflammatory markers [88]. In line with our results, kaempferol and quercetin are considered competitors for the IKKB ATP-binding pocket explaining their inhibitory activity on NF-κB pathway in other conditions [89,90]. Conversely, the potential molecular interactions of apigenin, 7-O-methylchrysin and isoquercetin with IKKB have not been previously reported and deserve further investigation.

Overall, our data suggest that *EQ* might delay the onset of OS in mice by acting directly on bone and muscle tissues, and indirectly on spleen-related inflammaging [41]. Indeed, we found that *EQ* strongly restrains age-related spleen microanatomy disruption and inflammation, preserving spleen size, reducing the number of giant cells and pro-inflammatory cytokines production, and limiting the expansion of macrophages. These results are in line with published data showing the anti-inflammatory capability of *EQ* in several immune cells [91]. Furthermore, in obesity-induced skeletal muscle atrophy apigenin treatment increased muscle mass, fiber size, and exercise capacity by suppressing the levels of inflammatory cytokines (TNF-α, IL-6, and IL-1) in serum and muscle tissue, in accordance with *EQ* effects in old mice [92]. Notably, apigenin, kaempferol, and 3′,4′-dichloroflavone are considered the best flavonoids able to reduce the production of IL-1β [93], which results down-regulated by *EQ* administration in both serum and muscle tissues, suggesting that *EQ* could interrupt pro-inflammaging status deriving by both spleen and myokine secretion thanks to flavonoid content.

Further investigations could consolidate our findings to include the supplement of *EQ* inside a multidimensional clinical approach for the prevention of OS onset and progression, considering that no toxicity was detected in our and others' studies [94]

5. Conclusions

Collectively, our data identify *EQ* as the first natural compound to simultaneously preserve muscle functionality and bone microarchitecture restraining the age-related modification in both tissues and by reducing the inflammatory state in muscle and spleen. We showed

that *EQ* has anti-atrophic and anti-osteoclastogenic activities *in vitro* blunting the deleterious effects of common risk factors for osteoporosis and sarcopenia, *i.e.*, inflammaging, excess of glucocorticoids and unbalanced release of the RANKL osteokine. Moreover, *EQ* maintains muscle size and strength, and bone structure during aging. In addition to silica, targeted UHPLC-MS profiling of our *EQ* extract provided a coexistence of multiple metabolites with already demonstrated properties in muscle and bone tissues justifying its beneficial effects on osteosarcopenic experimental models. *In silico* analyses provide the opportunity to investigate new molecular pathways underlying the *EQ* biological effects. Based on our promising results, further pre-clinical and clinical studies should be performed to evaluate the absorption extent, bioavailability, and efficacy of *EQ* extract. As a result, developing a low-cost food supplement emerges as a promising intervention for addressing OS, a pressing and unresolved health concern exacerbated by increasing life expectancy.

Ethical approval

Approval was granted by the Ethics Committee of the University of Perugia and the Italian Ministry of Health.

Funding

The authors were supported by Fondazione Cassa di Risparmio di Perugia (Project 2019.0321.026 to G.S.), by the AGING Project "Departments of Excellence 2018–2022", DIMET (L.S. and N.F.), by PRIN2022 (Prot. 2022B8KE33) to G.S. L.S. was supported by Fondazione Veronesi.

CRediT authorship contribution statement

Maria Letizia Barreca: Data curation, Methodology, Software. **Andrea Astolfi:** Formal analysis, Methodology. **Michela Bosetti:** Writing – review & editing, Supervision. **Beatrice Castiglioni:** Investigation, Formal analysis. **Leonardo Tensi:** Methodology, Formal analysis. **Martina Paiella:** Investigation, Formal analysis. **Roccaldo Sardella:** Methodology, Formal analysis. **Laura Salvadori:** Writing – original draft, Investigation, Formal analysis, Data curation. **Giulia Gentili:** Formal analysis. **Francesca Riuzzi:** Writing – review & editing, Supervision, Conceptualization. **Sara Chiappalupi:** Formal analysis. **Andrea Scircoli:** Formal analysis. **Nausicaa Clemente:** Formal analysis. **Luca Cornioli:** Resources. **Catia Ercolani:** Resources. **Nicoletta Filigheddu:** Writing – review & editing, Supervision, Project administration, Funding acquisition. **Tommaso Manenti:** Resources. **Guglielmo Sorci:** Writing – review & editing, Supervision, Project administration, Funding acquisition. **Maria Laura Belladonna:** Writing – review & editing, Investigation, Formal analysis, Data curation.

Declaration of Competing Interest

The authors declare that they have no known competing financial interests or personal relationships that could have appeared to influence the work reported in this paper.

Data availability

Data will be made available on request.

Acknowledgments

Not applicable.

Consent for publication

Publication of the manuscript has been approved by all co-authors.

Appendix A. Supporting information

Supplementary data associated with this article can be found in the online version at doi:10.1016/j.biopha.2024.116517.

References

[1] B. Kirk, J. Zanker, G. Duque, Osteosarcopenia: epidemiology, diagnosis, and treatment-facts and numbers, J. Cachexia Sarcopenia Muscle 11 (2020) 609–618, https://doi.org/10.1002/jcsm.12567.
[2] T.J. Aspray, T.R. Hill, Osteoporosis and the ageing skeleton, Subcell. Biochem. 91 (2019) 453–476, https://doi.org/10.1007/978-981-13-3681-2_16.
[3] P. Wiedmer, T. Jung, J.P. Castro, L.C.D. Pomatto, P.Y. Sun, K.J.A. Davies, T. Grune, Sarcopenia - molecular mechanisms and open questions, Ageing Res. Rev. 65 (2021) 101200, https://doi.org/10.1016/j.arr.2020.101200.
[4] N. Binkley, B. Buehring, Beyond FRAX: it's time to consider "sarco-osteopenia, J. Clin. Densitom. 12 (2009) 413–416, https://doi.org/10.1016/j.jocd.2009.06.004.
[5] A. Polito, L. Barnaba, D. Ciarapica, E. Azzini, Osteosarcopenia: a narrative review on clinical studies, Int. J. Mol. Sci. 23 (2022) 5591, https://doi.org/10.3390/ijms23105591.
[6] G. Colaianni, G. Storlino, L. Sanesi, S. Colucci, M. Grano, Myokines and osteokines in the pathogenesis of muscle and bone diseases, Curr. Osteoporos. Rep. 18 (2020) 401–407, https://doi.org/10.1007/s11914-020-00600-8.
[7] M. Masłowski, J. Miedzianowska, A. Czylkowska, K. Strzelec, Horsetail (Equisetum arvense) as a functional filler for natural rubber biocomposites, Materials 13 (2020) 2526, https://doi.org/10.3390/ma13112526.
[8] G. Saudelli, L. Tinti, G. Suffritti, A review on the treatment of osteoporosis with equisetum arvense, Gen. Med. 6 (2) (2018), https://doi.org/10.4172/2327-5146.1000313.
[9] S. Chiappalupi, G. Sorci, A. Vukasinovic, L. Salvadori, R. Sagheddu, D. Coletti, G. Renga, L. Romani, R. Donato, F. Riuzzi, Targeting RAGE prevents muscle wasting and prolongs survival in cancer cachexia, J. Cachexia Sarcopenia Muscle 11 (2020) 929–946, https://doi.org/10.1002/jcsm.12561.
[10] C. Orabona, E. Orecchini, C. Volpi, F. Bacaloni, E. Panfili, C. Pagano, L. Perioli, M. L. Belladonna, Crocus sativus L. petal extract inhibits inflammation and osteoclastogenesis in RAW 264.7 cell model, Pharmaceutics 14 (2022) 1290, https://doi.org/10.3390/pharmaceutics14061290.
[11] E. Orecchini, G. Mondanelli, C. Orabona, C. Volpi, S. Adorisio, M. Calvitti, T. T. Thuy, D.V. Delfino, M.L. Belladonna, Artocarpus tonkinensis extract inhibits LPS-triggered inflammation markers and suppresses rankl-induced osteoclastogenesis in RAW264.7, Front. Pharmacol. 11 (2021) 593829, https://doi.org/10.3389/fphar.2020.593829.
[12] L. Salvadori, M. Mandrone, T. Manenti, C. Ercolani, L. Cornioli, M. Lianza, P. Tomasi, S. Chiappalupi, E.S. Di Filippo, S. Fulle, F. Poli, G. Sorci, F. Riuzzi, Identification of Withania somnifera-Silybum marianum-Trigonella foenum-graecum formulation as a nutritional supplement to contrast muscle atrophy and sarcopenia, Nutrients 13 (2020 Dec) 49, https://doi.org/10.3390/nu13010049.
[13] L. Salvadori, M.L. Belladonna, B. Castiglioni, M. Paiella, E. Panfili, T. Manenti, C. Ercolani, L. Cornioli, S. Chiappalupi, G. Gentili, M. Leigheb, G. Sorci, M. Bosetti, N. Filigheddu, F. Riuzzi, KYMASIN UP natural product inhibits osteoclastogenesis and improves osteoblast activity by modulating Src and p38 MAPK, Nutrients 14 (2022) 3053, https://doi.org/10.3390/nu14153053.
[14] M. Bosetti, A. Massè, E. Tobin, M. Cannas, In vivo evaluation of bone tissue behavior on ion implanted surfaces, J. Mater. Sci. Mater. Med. 12 (2001) 431–435, https://doi.org/10.1023/a:1011253121063.
[15] M.L. Bouxsein, S.K. Boyd, B.A. Christiansen, R.E. Guldberg, K.J. Jepsen, R. Müller, Guidelines for assessment of bone microstructure in rodents using micro-computed tomography, J. Bone Miner. Res. 25 (2010) 1468–1486, https://doi.org/10.1002/jbmr.141.
[16] Schrödinger Release -1: LigPrep, Schrödinger, LLC, New York, NY, 2024.
[17] H.M. Berman, T. Battistuz, T.N. Bhat, W.F. Bluhm, P.E. Bourne, K. Burkhardt, Z. Feng, G.L. Gilliland, L. Iype, S. Jain, P. Fagan, J. Marvin, D. Padilla, V. Ravichandran, B. Schneider, N. Thanki, H. Weissig, J.D. Westbrook, C. Zardecki, The protein data bank, Acta Crystallogr D Biol. Crystallogr. 58 (2002) 899–907, https://doi.org/10.1107/s0907444902003451.
[18] Schrödinger Release 2024–1: Protein Preparation Wizard.
[19] Epik, Schrödinger, LLC, New York, NY, 2024.
[20] Impact, Schrödinger, LLC, New York, NY.
[21] Prime, Schrödinger, LLC, New York, NY, 2024.
[22] C. Lu, C. Wu, D. Ghoreishi, W. Chen, L. Wang, W. Damm, G.A. Ross, M.K. Dahlgren, E. Russell, C.D. Von Bargen, R. Abel, R.A. Friesner, E.D. Harder, OPLS4: improving force field accuracy on challenging regimes of chemical space, J. Chem. Theory Comput. 17 (2021) 4291–4300, https://doi.org/10.1021/acs.jctc.1c00302.
[23] Schrödinger Release -1: Glide, Schrödinger, LLC, New York, NY, 2024.
[24] R.A. Friesner, J.L. Banks, R.B. Murphy, T.A. Halgren, J.J. Klicic, D.T. Mainz, M. P. Repasky, E.H. Knoll, D.E. Shaw, M. Shelley, J.K. Perry, P. Francis, P.S. Shenkin, Glide: A new approach for rapid, accurate docking and scoring. 1. Method and assessment of docking accuracy, J. Med. Chem. 47 (2004) 1739–1749.
[25] R. Sartori, V. Romanello, M. Sandri, Mechanisms of muscle atrophy and hypertrophy: implications in health and disease, Nat. Commun. 12 (2021) 330, https://doi.org/10.1038/s41467-020-20123-1.

[26] M. Christian, W.B. Hannah, H. Lüthen, A.M. Jones, Identification of auxins by a chemical genomics approach, J. Exp. Bot. 59 (2008) 2757–2767, https://doi.org/10.1093/jxb/ern133.
[27] L. Marcadet, Z. Bouredji, A. Argaw, J. Frenette, The roles of RANK/RANKL/OPG in cardiac, skeletal, and smooth muscles in health and disease, Front. Cell Dev. Biol. 10 (2022) 903657, https://doi.org/10.3389/fcell.2022.903657.
[28] J. Chal, O. Pourquié, Making muscle: skeletal myogenesis in vivo and in vitro, Development 144 (2017) 2104–2122, https://doi.org/10.1242/dev.151035.
[29] J.F. Ma, B.J. Sanchez, D.T. Hall, A.K. Tremblay, S. Di Marco, I.E. Gallouzi, STAT3 promotes IFNγ/TNFα-induced muscle wasting in an NF-κB-dependent and IL-6-independent manner, EMBO Mol. Med. 9 (2017) 622–637, https://doi.org/10.15252/emmm.201607052.
[30] W. Chamberlain, P. Gonnella, N. Alamdari, Z. Aversa, P.O. Hasselgren, Multiple muscle wasting-related transcription factors are acetylated in dexamethasone-treated muscle cells, Biochem. Cell Biol. 90 (2012) 200–208, https://doi.org/10.1139/o11-082.
[31] L. Nogueira, E.C. Breen, Cigarettes make you weak: RANKL/RANK link changes in muscle and bone, Am. J. Respir. Cell Mol. Biol. 64 (2021) 533–535, https://doi.org/10.1165/rcmb.2021-0098ED.
[32] J. Xiong, Y. Le, Y. Rao, L. Zhou, Y. Hu, S. Guo, Y. Sun, RANKL mediates muscle atrophy and dysfunction in a cigarette smoke-induced model of chronic obstructive pulmonary disease, Am. J. Respir. Cell Mol. Biol. 64 (2021) 617–628, https://doi.org/10.1165/rcmb.2020-0449OC.
[33] S.D. Kotwal, S.R. Badole, Anabolic therapy with Equisetum arvense along with bone mineralising nutrients in ovariectomized rat model of osteoporosis, Indian J. Pharmacol. 48 (2016) 312–315, https://doi.org/10.4103/0253-7613.182880.
[34] H. Li, J. Wang, Q. Sun, G. Chen, S. Sun, X. Ma, H. Qiu, X. Liu, L. Xu, M. Liu, Jatrorrhizine hydrochloride suppresses RANKL-induced osteoclastogenesis and protects against wear particle-induced osteolysis, Int. J. Mol. Sci. 19 (2018) 3698, https://doi.org/10.3390/ijms19113698.
[35] W.Q. Xie, M. He, D.J. Yu, Y.X. Wu, X.H. Wang, S. Lv, W.F. Xiao, Y.S. Li, Mouse models of sarcopenia: classification and evaluation, J. Cachexia Sarcopenia Muscle 12 (2021) 538–554, https://doi.org/10.1002/jcsm.12709.
[36] I.H. Lin, J.L. Chang, K. Hua, W.C. Huang, M.T. Hsu, Y.F. Chen, Skeletal muscle in aged mice reveals extensive transformation of muscle gene expression, BMC Genet. 19 (2018) 55, https://doi.org/10.1186/s12863-018-0660-5.
[37] V.L. Ferguson, R.A. Ayers, T.A. Bateman, S.J. Simske, Bone development and age-related bone loss in male C57BL/6J mice, Bone 33 (2003) 387–398, https://doi.org/10.1016/s8756-3282(03)00199-6.
[38] K.M. Delahunty, L.G. Horton, H.F. Coombs 3rd, K.L. Shultz, K.L. Svenson, M. A. Marion, M.F. Holick, W.G. Beamer, C.J. Rosen, Gender- and compartment-specific bone loss in C57BL/6J mice: correlation to season, J. Clin. Densitom. 12 (2009) 89–94, https://doi.org/10.1016/j.jocd.2008.10.008.
[39] X. Lin, S. Patil, Y.G. Gao, A. Qian, The bone extracellular matrix in bone formation and regeneration, Front. Pharmacol. 11 (2020) 757, https://doi.org/10.3389/fphar.2020.00757.
[40] S. Boyd, R. Müller. Microimaging. Principles of Bone Biology (Fourth Edition), Academic Press, 2020, pp. 1833–1856, 79.
[41] D. Aw, L. Hilliard, Y. Nishikawa, E.T. Cadman, R.A. Lawrence, D.B. Palmer, Disorganization of the splenic microanatomy in ageing mice, Immunology 148 (2016) 92–101, https://doi.org/10.1111/imm.12590.
[42] Zia-Ur-Rehman, A. Gurgul, I. Youn, A. Maldonado, F. Wahid, C.T. Che, T. Khan, UHPLC-MS/MS-GNPS based phytochemical investigation of Equisetum arvense L. And evaluation of cytotoxicity against human melanoma and ovarian cancer cells, Saudi J. Biol. Sci. 29 (2022) 103271, https://doi.org/10.1016/j.sjbs.2022.03.021.
[43] P. Songkiatisak, S.M.T. Rahman, M. Aqdas, M.H. Sung, NF-κB, a culprit of both inflamm-ageing and declining immunity? Immun. Ageing 19 (2022) 20, https://doi.org/10.1186/s12979-022-00277-w.
[44] F. Ciriaco, N. Gambacorta, D. Trisciuzzi, O. Nicolotti, PLATO: a predictive drug discovery web platform for efficient target fishing and bioactivity profiling of small molecules, Int. J. Mol. Sci. 23 (2022) 5245, https://doi.org/10.3390/ijms23095245.
[45] D. Mendez, A. Gaulton, A.P. Bento, J. Chambers, M. De Veij, E. Félix, M. P. Magariños, J.F. Mosquera, P. Mutowo, M. Nowotka, M. Gordillo-Marañón, F. Hunter, L. Junco, G. Mugumbate, M. Rodriguez-Lopez, F. Atkinson, N. Bosc, C. J. Radoux, A. Segura-Cabrera, A. Hersey, A.R. Leach, ChEMBL: towards direct deposition of bioassay data, Nucleic Acids Res. 47 (2019) D930–D940, https://doi.org/10.1093/nar/gky1075.
[46] A. Paul, J. Edwards, C. Pepper, S. Mackay, Inhibitory-κB kinase (IKK) α and nuclear factor-κB (NFκB)-inducing kinase (NIK) as anti-cancer drug targets, Cells 7 (2018) 176, https://doi.org/10.3390/cells7100176.
[47] Y. Hou, F. Moreau, K. Chadee, PPARγ is an E3 ligase that induces the degradation of NFκB/p65, Nat. Commun. 3 (2012) 1300, https://doi.org/10.1038/ncomms2270.
[48] S. Pasquini, C. Contri, P.A. Borea, F. Vincenzi, K. Varani, Adenosine and inflammation: here, there and everywhere, Int. J. Mol. Sci. 22 (2021) 7685, https://doi.org/10.3390/ijms22147685.
[49] Y. Fan, R. Mao, J. Yang, NF-κB and STAT3 signaling pathways collaboratively link inflammation to cancer, Protein Cell 4 (2013) 176–185, https://doi.org/10.1007/s13238-013-2084-3.
[50] L. Ghoda, X. Lin, W.C. Greene, The 90-kDa ribosomal S6 kinase (pp90rsk) phosphorylates the N-terminal regulatory domain of IkappaBalpha and stimulates its degradation in vitro, J. Biol. Chem. 272 (1997) 21281–21288, https://doi.org/10.1074/jbc.272.34.21281.
[51] C.H. Régnier, H.Y. Song, X. Gao, D.V. Goeddel, Z. Cao, M. Rothe, Identification and characterization of an IkappaB kinase, Cell 90 (1997) 373–383, https://doi.org/10.1016/s0092-8674(00)80344-x.
[52] A. Bastin, M. Teimouri, S. Faramarz, M. Shabani, A.H. Doustimotlagh, A. Sadeghi, In vitro and molecular docking analysis of quercetin as an anti-inflammatory and antioxidant, Curr. Pharm. Des. 29 (2023) 883–891, https://doi.org/10.2174/1381612829666230330084043.
[53] M. Bagherniya, A. Mahdavi, N. Shokri-Mashhadi, M. Banach, S. Von Haehling, T. P. Johnston, A. Sahebkar, The beneficial therapeutic effects of plant-derived natural products for the treatment of sarcopenia, J. Cachexia Sarcopenia Muscle (2022) 132772–132790, https://doi.org/10.1002/jcsm.13057.
[54] S.A. Harper, J.R. Bassler, S. Peramsetty, Y. Yang, L.M. Roberts, D. Drummer, R. T. Mankowski, C. Leeuwenburgh, K. Ricart, R.P. Patel, M.M. Bamman, S.D. Anton, B.C. Jaeger, T.W. Buford, Resveratrol and exercise combined to treat functional limitations in late life: a pilot randomized controlled trial, Exp. Gerontol. 143 (2021) 111111, https://doi.org/10.1016/j.exger.2020.111111.
[55] H. Kim, T. Suzuki, K. Saito, H. Yoshida, N. Kojima, M. Kim, M. Sudo, Y. Yamashiro, I. Tokimitsu, Effects of exercise and tea catechins on muscle mass, strength and walking ability in community-dwelling elderly Japanese sarcopenic women: a randomized controlled trial, Geriatr. Gerontol. Int. 13 (2013) 458–465, https://doi.org/10.1111/j.1447-0594.2012.00923.x.
[56] D. Lee, A.L. Goldberg, Muscle wasting in fasting requires activation of NF-κB and inhibition of AKT/mechanistic target of rapamycin (mTOR) by the protein acetylase, GCN5, J. Biol. Chem. 290 (2015) 30269–30279, https://doi.org/10.1074/jbc.M115.685164.
[57] R. Manickam, K. Duszka, W. Wahli, PPARs and microbiota in skeletal muscle health and wasting, Int. J. Mol. Sci. 21 (2020) 8056, https://doi.org/10.3390/ijms21218056.
[58] M. Marabita, M. Baraldo, F. Solagna, J.J.M. Ceelen, R. Sartori, H. Nolte, I. Nemazanyy, S. Pyronnet, M. Kruger, M. Pende, B. Blaauw, S6K1 is required for increasing skeletal muscle force during hypertrophy, Cell Rep. 17 (2016) 501–513, https://doi.org/10.1016/j.celrep.2016.09.020.
[59] R. Nilwik, T. Snijders, M. Leenders, B.B. Groen, J. van Kranenburg, L.B. Verdijk, L. J. van Loon, The decline in skeletal muscle mass with aging is mainly attributed to a reduction in type II muscle fiber size, Exp. Gerontol. 48 (2013) 492–498, https://doi.org/10.1016/j.exger.2013.02.012.
[60] J. Costa-Rodrigues, S.C. Carmo, J.C. Silva, M.H. Fernandes, Inhibition of human in vitro osteoclastogenesis by Equisetum arvense, Cell Prolif. 45 (2012) 566–576, https://doi.org/10.1111/j.1365-2184.2012.00848.x.
[61] W. He, B.N. Cronstein, Adenosine A1 receptor regulates osteoclast formation by altering TRAF6/TAK1 signaling, Purinergic Signal. 8 (2012) 327–337, https://doi.org/10.1007/s11302-012-9292-9.
[62] J. Cao, L. Venton, T. Sakata, B.P. Halloran, Expression of RANKL and OPG correlates with age-related bone loss in male C57BL/6 mice, J. Bone Miner. Res. 18 (2003) 270–277, https://doi.org/10.1359/jbmr.2003.18.2.270.
[63] C. Bessa Pereira, P.S. Gomes, J. Costa-Rodrigues, R. Almeida Palmas, L. Vieira, M. P. Ferraz, M.A. Lopes, M.H. Fernandes, Equisetum arvense hydromethanolic extracts in bone tissue regeneration: in vitro osteoblastic modulation and antibacterial activity, Cell Prolif. 45 (2012) 386–396, https://doi.org/10.1111/j.1365-2184.2012.00826.x.
[64] J. Lappe, I. Kunz, I. Bendik, K. Prudence, P. Weber, R. Recker, R.P. Heaney, Effect of a combination of genistein, polyunsaturated fatty acids and vitamins D3 and K1 on bone mineral density in postmenopausal women: a randomized, placebo-controlled, double-blind pilot study, Eur. J. Nutr. 52 (2013) 203–215, https://doi.org/10.1007/s00394-012-0304-x.
[65] V. Arcoraci, M. Atteritano, F. Squadrito, R. D'Anna, H. Marini, D. Santoro, L. Minutoli, S. Messina, D. Altavilla, A. Bitto, Antiosteoporotic activity of genistein aglycone in postmenopausal women: evidence from a post-hoc analysis of a multicenter randomized controlled trial, Nutrients 9 (2017) 179, https://doi.org/10.3390/nu9020179.
[66] A.M. Keiler, D. Macejova, B.M. Dietz, J.L. Bolton, G.F. Pauli, S.N. Chen, R.B. van Breemen, D. Nikolic, F. Goerl, M.H. Muders, O. Zierau, G. Vollmer, Evaluation of estrogenic potency of a standardized hops extract on mammary gland biology and on MNU-induced mammary tumor growth in rats, J. Steroid Biochem. Mol. Biol. 174 (2017) 234–241, https://doi.org/10.1016/j.jsbmb.2017.09.020.
[67] P. Ramesh, R. Jagadeesan, S. Sekaran, A. Dhanasekaran, S. Vimalraj, Flavonoids: classification, function, and molecular mechanisms involved in bone remodelling, Front. Endocrinol. 12 (2021) 779638, https://doi.org/10.3389/fendo.2021.779638.
[68] J.T. Woo, H. Nakagawa, M. Notoya, T. Yonezawa, N. Udagawa, I.S. Lee, M. Ohnishi, H. Hagiwara, K. Nagai, Quercetin suppresses bone resorption by inhibiting the differentiation and activation of osteoclasts, Biol. Pharm. Bull. 27 (2004) 504–509, https://doi.org/10.1248/bpb.27.504.
[69] S.K. Wong, K.Y. Chin, S. Ima-Nirwana, The osteoprotective effects of kaempferol: the evidence from in vivo and in vitro studies, Drug Des. Dev. Ther. 13 (2019) 3497–3514, https://doi.org/10.2147/DDDT.S227738.
[70] T. Goto, K. Hagiwara, N. Shirai, K. Yoshida, H. Hagiwara, Apigenin inhibits osteoblastogenesis and osteoclastogenesis and prevents bone loss in ovariectomized mice, Cytotechnology 67 (2015) 357–365, https://doi.org/10.1007/s10616-014-9694-3.
[71] J.A. Park, S.K. Ha, T.H. Kang, M.S. Oh, M.H. Cho, S.Y. Lee, J.H. Park, S.Y. Kim, Protective effect of apigenin on ovariectomy-induced bone loss in rats, Life Sci. 82 (2008) 1217–1223, https://doi.org/10.1016/j.lfs.2008.03.021.
[72] T. Sagar, M. Rantlha, M.C. Kruger, M. Coetzee, V. Deepak, Ferulic acid impairs osteoclast fusion and exacerbates survival of mature osteoclasts, Cytotechnology 68 (2016) 1963–1972, https://doi.org/10.1007/s10616-016-0009-8.

[73] H.M. Doss, S. Samarpita, R. Ganesan, M. Rasool, Ferulic acid, a dietary polyphenol suppresses osteoclast differentiation and bone erosion via the inhibition of RANKL dependent NF-κB signalling pathway, Life Sci. 207 (2018) 284–295, https://doi.org/10.1016/j.lfs.2018.06.013.
[74] T. Hou, L. Zhang, X. Yang, Ferulic acid, a natural polyphenol, protects against osteoporosis by activating SIRT1 and NF-κB in neonatal rats with glucocorticoid-induced osteoporosis, Biomed. Pharmacother. 120 (2019) 109205, https://doi.org/10.1016/j.biopha.2019.109205.
[75] X. Fu, X. Sun, C. Zhang, N. Lv, H. Guo, C. Xing, J. Lv, J. Wu, X. Zhu, M. Liu, L. Su, Genkwanin prevents lipopolysaccharide-induced inflammatory bone destruction and ovariectomy-induced bone loss, Front. Nutr. 9 (2022) 921037, https://doi.org/10.3389/fnut.2022.921037.
[76] T. Nikawa, A. Ulla, I. Sakakibara, Polyphenols and their effects on muscle atrophy and muscle health, Molecules 26 (2021) 4887, https://doi.org/10.3390/molecules26164887.
[77] Y. Kim, C.S. Kim, Y. Joe, H.T. Chung, T.Y. Ha, R. Yu, Quercetin reduces tumor necrosis factor alpha-induced muscle atrophy by upregulation of heme oxygenase-1, J. Med. Food 21 (2018) 551–559, https://doi.org/10.1089/jmf.2017.4108.
[78] C. Chen, J.S. Yang, C.C. Lu, Y.J. Chiu, H.C. Chen, M.I. Chung, Y.T. Wu, F.A. Chen, Effect of quercetin on dexamethasone-induced C2C12 skeletal muscle cell injury, Molecules 25 (2020) 3267, https://doi.org/10.3390/molecules25143267.
[79] N.H. Le, C.S. Kim, T. Park, J.H. Park, M.K. Sung, D.G. Lee, S.M. Hong, S.Y. Choe, T. Goto, T. Kawada, R. Yu, Quercetin protects against obesity-induced skeletal muscle inflammation and atrophy, Mediat. Inflamm. 2014 (2014) 834294, https://doi.org/10.1155/2014/834294.
[80] R. Mukai, R. Nakao, H. Yamamoto, T. Nikawa, E. Takeda, J. Terao, Quercetin prevents unloading-derived disused muscle atrophy by attenuating the induction of ubiquitin ligases in tail-suspension mice, J. Nat. Prod. 73 (2010) 1708–1710, https://doi.org/10.1021/np100240y.
[81] Y. Otsuka, K. Egawa, N. Kanzaki, T. Izumo, T. Rogi, H. Shibata, Quercetin glycosides prevent dexamethasone-induced muscle atrophy in mice, Biochem. Biophys. Rep. 11 (18) (2019) 100618, https://doi.org/10.1016/j.bbrep.2019.100618.
[82] N. Kanzaki, D. Takemoto, Y. Ono, T. Izumo, H. Shibata, X. Ye, Quercetin glycosides improve motor performance and muscle weight in adult mice, J. Nutr. Food Sci. 9 (2019). ISSN: 2155-9600.
[83] D. Wang, Y. Yang, X. Zou, J. Zhang, Z. Zheng, Z. Wang, Antioxidant apigenin relieves age-related muscle atrophy by inhibiting oxidative stress and hyperactive mitophagy and apoptosis in skeletal muscle of mice, J. Gerontol. A Biol. Sci. Med. Sci. 75 (2020) 2081–2088, https://doi.org/10.1093/gerona/glaa214.
[84] Y.J. Jang, H.J. Son, Y.M. Choi, J. Ahn, C.H. Jung, T.Y. Ha, Apigenin enhances skeletal muscle hypertrophy and myoblast differentiation by regulating Prmt7, Oncotarget 8 (2017) 78300–78311, https://doi.org/10.18632/oncotarget.20962.
[85] W.H. Choi, Y.J. Jang, H.J. Son, J. Ahn, C.H. Jung, T.Y. Ha, Apigenin inhibits sciatic nerve denervation-induced muscle atrophy, Muscle Nerve 58 (2018) 314–318, https://doi.org/10.1002/mus.26133.
[86] M. Shereen, M.D. Samir, F. Abeer, M.D. Mostafa, Ferulic acid promotes growth of both fast glycolytic and slow oxidative skeletal muscles in corticosteroid-induced rat myopathy, Med. J. Cairo Univ. 44 (2019) 1703–1715, https://doi.org/10.21608/MJCU.2019.53950.
[87] Y. Wen, H. Ushio, Ferulic acid promotes hypertrophic growth of fast skeletal muscle in zebrafish model, Nutrients 9 (2017) 1066, https://doi.org/10.3390/nu9101066.
[88] Y.W. Sun, Y. Bao, H. Yu, Q.J. Chen, F. Lu, S. Zhai, C.F. Zhang, F. Li, C.Z. Wang, C. S. Yuan, Anti-rheumatoid arthritis effects of flavonoids from Daphne genkwa, Int. Immunopharmacol. 83 (2020) 106384, https://doi.org/10.1016/j.intimp.2020.106384.
[89] O. Kadioglu, J. Nass, M.E. Saeed, B. Schuler, T. Efferth, Kaempferol is an anti-inflammatory compound with activity towards NF-κB pathway proteins, Anticancer Res. 35 (2015) 2645–2650. PMID: 25964540.
[90] C.M. Avila, N.C. Romeiro, C.M. Sant'Anna, E.J. Barreiro, C.A. Fraga, Structural insights into IKKbeta inhibition by natural products staurosporine and quercetin. Bioorg. Med. Chem. Lett. 19 (2009) 6907–6910, https://doi.org/10.1016/j.bmcl.2009.10.076.
[91] C. Gründemann, K. Lengen, B. Sauer, M. Garcia-Käufer, M. Zehl, R. Huber, Equisetum arvense (common horsetail) modulates the function of inflammatory immunocompetent cells, BMC Complement. Altern. Med. 14 (2014) 283, https://doi.org/10.1186/1472-6882-14-283.
[92] W.H. Choi, H.J. Son, Y.J. Jang, J. Ahn, C.H. Jung, T.Y. Ha, Apigenin ameliorates the obesity-induced skeletal muscle atrophy by attenuating mitochondrial dysfunction in the muscle of obese mice, Mol. Nutr. Food Res. 61 (2017), https://doi.org/10.1002/mnfr.201700218.
[93] H. Lim, M.Y. Heo, H.P. Kim, Flavonoids: broad spectrum agents on chronic inflammation, Biomol. Ther. 27 (2019) 241–253, https://doi.org/10.4062/biomolther.2019.034.
[94] Y. Tago, M. Wei, N. Ishii, A. Kakehashi, H. Wanibuchi, Evaluation of the subchronic toxicity of dietary administered Equisetum arvense in F344 rats, J. Toxicol. Pathol. 23 (2010) 245–251, https://doi.org/10.1293/tox.23.245.